HIAPER Cloud Radar Ground-based Prototype

Gordon Farquharson, Peisang Tsai
National Center for Atmospheric Research
Boulder, CO

July 22, 2010

1 Introduction

This document details the design for the ground-based dual-antenna cloud radar prototype which will become the HIAPER Cloud Radar (HCR). Section 2 presents an overview of the transceiver design including the system block diagram. The theory of operation and description of the up- and down-conversion electronics are presented in Sections 3, 4 and 5 respectively. Section 6 presents methods used in HCR design to monitor system performance, the calibration target design, and measurements made during the prototype development. Section 7 summarizes the system performance this ground-based prototype configuration. Two sample observations were obtained in Section 8 to demonstrate HCR's capability in reflectivity and velocity measurements. Finally, summary of the achievement during this development is concluded in Section 9.

More in depth analysis on the transceiver design are introduced in Appendix. Appendix A outlines the decisions made in selecting the second stage intermediate frequency in the transceiver. The design and simulation of the waveform generator is presented in Appendix B.

2 System Overview

A system diagram of the ground-based, single-wavelength, dual-antenna HIAPER Cloud Radar (HCR) is shown in Figure 1. The HCR system includes four parts: data acquisition, IF, RF and klystron transmitter subsystem.

The data acquisition subsystem is comprised of a single-board computer, a digital receiver card and a data archiver computer. The single-board computer hosts the digital receiver and provides means for data archiving. A consumer-ready digital receiver and waveform generation card, Pentek 7142, is used for data acquisition and waveform generation. It receives a 125MHz reference clock from the transceiver and generates a transmit waveform at intermediate frequency (TX IN). This transmit waveform is further converted to the desired transmit frequency in the transceiver subsystem. The digital receiver

also digitizes two receive IF channels (TX CAL IF and RX IF) and generates time series radar data. Time series data is streamed to data archiver computer via Ethernet.

The klystron transmitter requires a high-voltage power supply modulator and a control and monitor unit for operation. The control and monitor unit provides control signals to the power supply modulator, receives status from the power supply, monitors the operation, as well as observes optical signal for klystron arc detection. The power supply generates high voltages to excite klystron transmitter.

The HCR transceiver is divided into RF and IF subsystems. The details of each subsystem will be described in Section 3.

2.1 Mechanical Layout

For the ground-based prototype configuration, HCR is installed on a sea container platform as shown in Figure 2. The transmit and receiver antenna are mounted on top of the container and RF front-end recedes inwards to be accessible to the rest of the system. A reflector panel is implemented for azimuthal observations. Inside the container resides data acquisition and klystron transmitter subsystems and workspace for radar operators.

Figure 3 demonstrates the initial antenna and RF front-end assembly. RF subsystem and power supply modulator are mounted below both antennas for minimum signal paths. When the initial layout was designed, two different aperture antenna were used. As the transmit antenna became unavailable, it is replaced with a 12" cassegrain reflector. The current configuration utilies two 12" cassegrain antenna. The receive antenna is mounted on three parallel plates to provide fine adjustments in azimuthal plane for antenna alignment.

Two custom-made shrouds were designed to provide additional isolation between transmit and receive. A 1-inch layer of millimeter-wave absorber is attached to the inner wall of the shrouds for microwave absorption. Both shroud tops are sealed with a low-loss millimeter-wave radome material for weather-proofing. In order to minimize signal paths and simplify system implementation, signals are converted to the second intermediate frequency, 1406.25 MHz, in RF front-end assembly. This allows simply four IF signal cables connecting between RF front-end and IF subsystem and also achieves low noise and low loss environment.

3 Theory of Operation

A block diagram of the transceiver is shown in Figure 4. The transceiver consists of three main sections: the electronics to up-convert the transmitted signal from the intermediate frequency to W-band; the electronics to down-convert the W-band received signal to the intermediate frequency; and a down-conversion channel to sample the transmitted waveform. The transceiver uses a two-stage up- and down-conversion super-heterodyne design. The first stage intermediate frequency is 156.25 MHz and the second stage intermediate frequency is 1406.25 MHz. A 10 MHz GPS STALO is used as the system coherent reference as well as the GPS coordinate and time reference. The system clock, 125 MHz, is referenced to the 10 MHz GPS STALO. Two antennas are used in this system to achieve isolation between the transmitter and receiver. Both antennas have matching 3-dB beamwidth of 0.68°. Nominal signal levels are shown in Figure 4. The radar specifications are listed in Table 2.

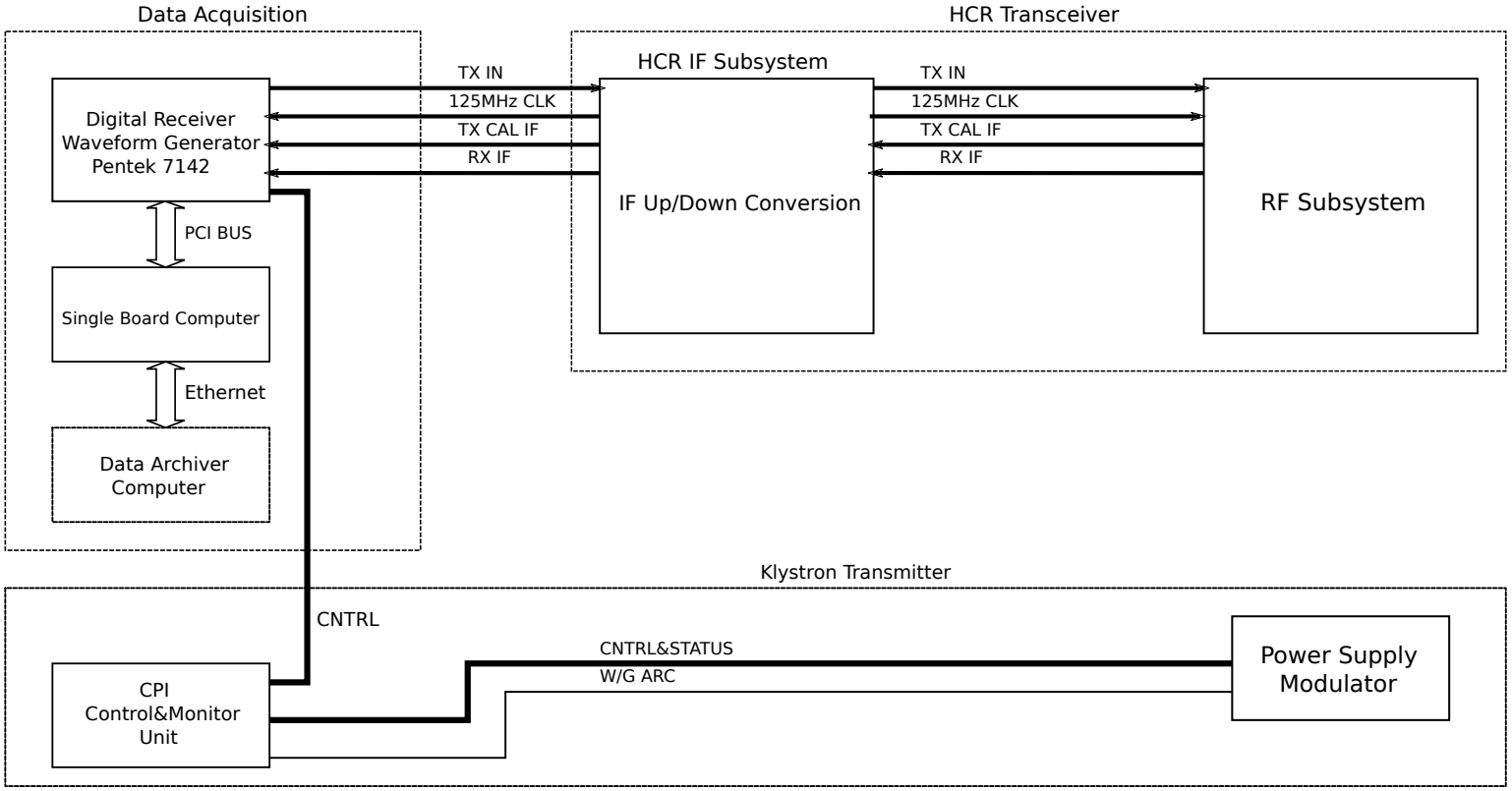

Figure 1: Ground-based system diagram

Figure 2: HCR ground-based sea container platform.

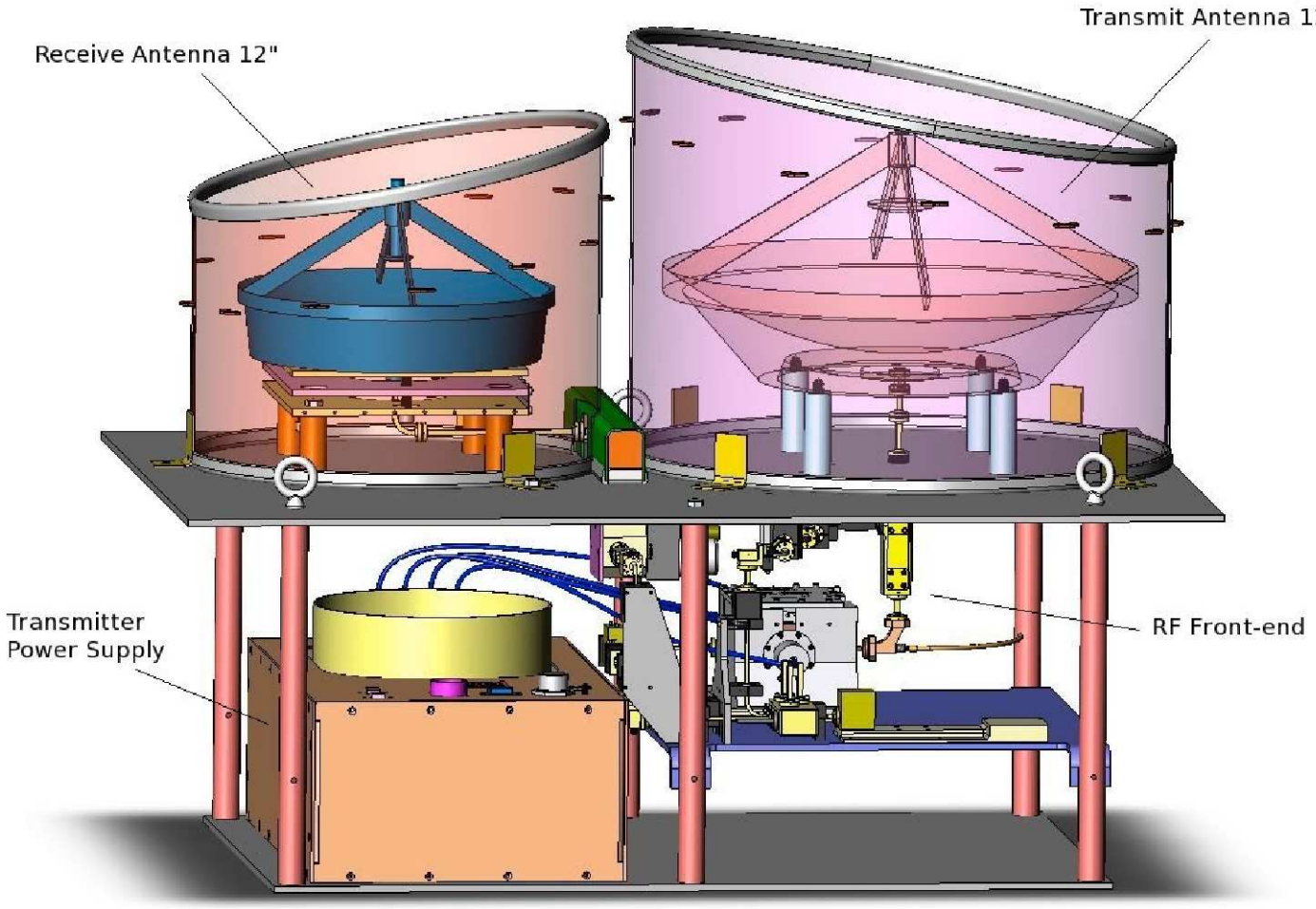

Figure 3: Ground-based system mechanical layout

The receiver bandwidth is determined by the minimum range resolution specification (30 meters). For a pulse width of 200 ns, the bandwidth is 5 MHz. The receiver bandwidths are specified for a minimum 20 MHz pass band to accommodate lower range resolutions. The sensitivity of the system will be optimized to the pulse length used by digitally filtering the received signal to desired signal bandwidth after digitization. The intermediate frequency and analog to digital sampling rate selected for the radar are 156.25 MHz and 125 MS/s respectively. Details about the selection of intermediate frequency are listed in the Appendix A. An intermediate frequency of 156.25 MHz, in conjunction with a sampling frequency of 125 MS/s, satisfies the $f_s/4$ demodulation scheme for narrow-band signals. A signal centered at 156.25 MHz will alias to 31.25 MHz when sampled at a rate of 125 MS/s, and 31.25 MHz is one quarter of 125 MHz as required.

4 Up-conversion Electronics

The up-conversion electronics in the transceiver are configured in a two-stage super-heterodyne configuration. Figure 5 shows a frequency domain representation of the signals implemented in the transceiver. The signal at the output of the waveform generator (156.25 MHz) is up converted to 1406.25 MHz using a single sideband modulator and then filtered to suppress the image frequency lower side band signal (1093.75 MHz). The signal at 1406.25 GHz is then up-converted to W-band (94.40625 GHz) with a W-band single-sideband modulator, and filtered before transmission. The choice of the local oscillator frequencies are such that they are integer multiples of the 125 MHz master oscillator.

4.1 Spectrum Analysis

The filter at the output of the waveform generator must suppress the spurious signals that are generated by the waveform generator. The transmitter spurious output level is specified to be less than 70 dB which means that we should suppress the spurious and harmonically generated signal from the waveform generator by at least this much.

The suppression at 93.75 MHz must be greater than 23 dB and at 218.25 MHz must be greater than 29 dB to suppress the non harmonically-generated spurious signal by greater than 70 dB. A Lorch bandpass filter is selected for the first stage IF filter. Table 1 shows the stopband characterestics easily exceed the suppression requirements.

Table 1: Lorch band pass filter stopband characteristics

Frequency MHz	4BP3-156.25/R20-S dB
93.75	75.9
125.00	35.1
187.5	15.1
218.75	31.6

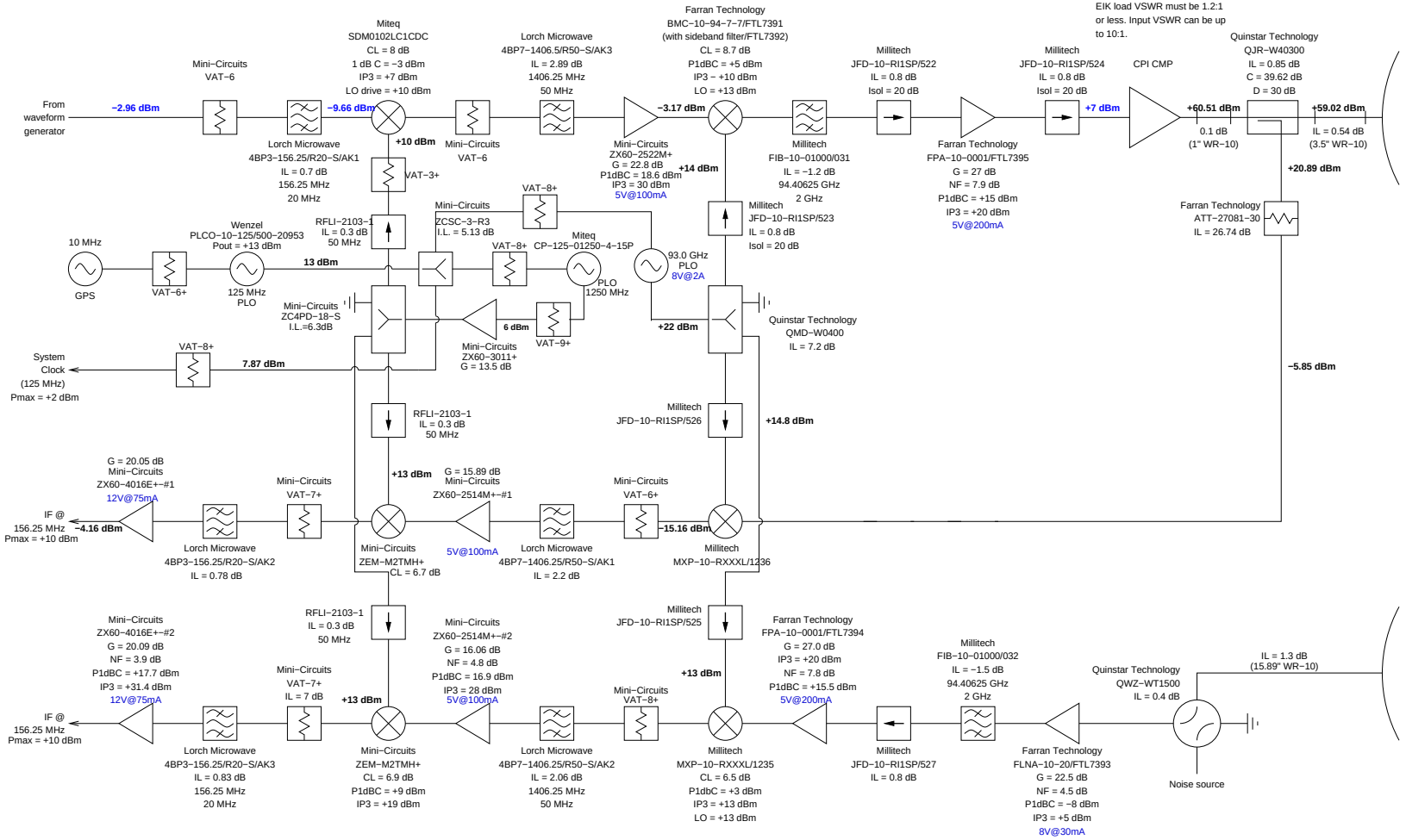

Figure 4: Transceiver block diagram.

Table 2: HIAPER Cloud Radar system specifications

Antenna Subsystem	
Transmit Reflector	
Type	Cassegrain
Diameter	0.3 m
Gain	46.21 dB
Beamwidth	0.68°
Transmit Frequency	94.40625 GHz
Receive Reflector	
Type	Cassegrain
Diameter	0.3 m
Gain	46.3 dB
Beamwidth	0.69°
Transmitter and receiver subsystem	
Transmitter	
Type	Klystron
Frequency	94.40625 GHz
Peak Power	1.6 kW
Pulse Width	200 ns - 1μs
Pulse Repetition Frequency	10 kHz
Receiver	
Receiver Noise Figure	8.9 dB
Receiver Dynamic Range	76 dB
Receiver Bandwidth	20 MHz
System Noise Power	-104 dBm
First IF	156.25 MHz
Second IF	1406.25 MHz
Sensitivity	-39.6 dBZ at 1 km, 0 dB SNR
Unambiguous Velocity	$\pm$7.75 m/s
Dwell Time	100 ms

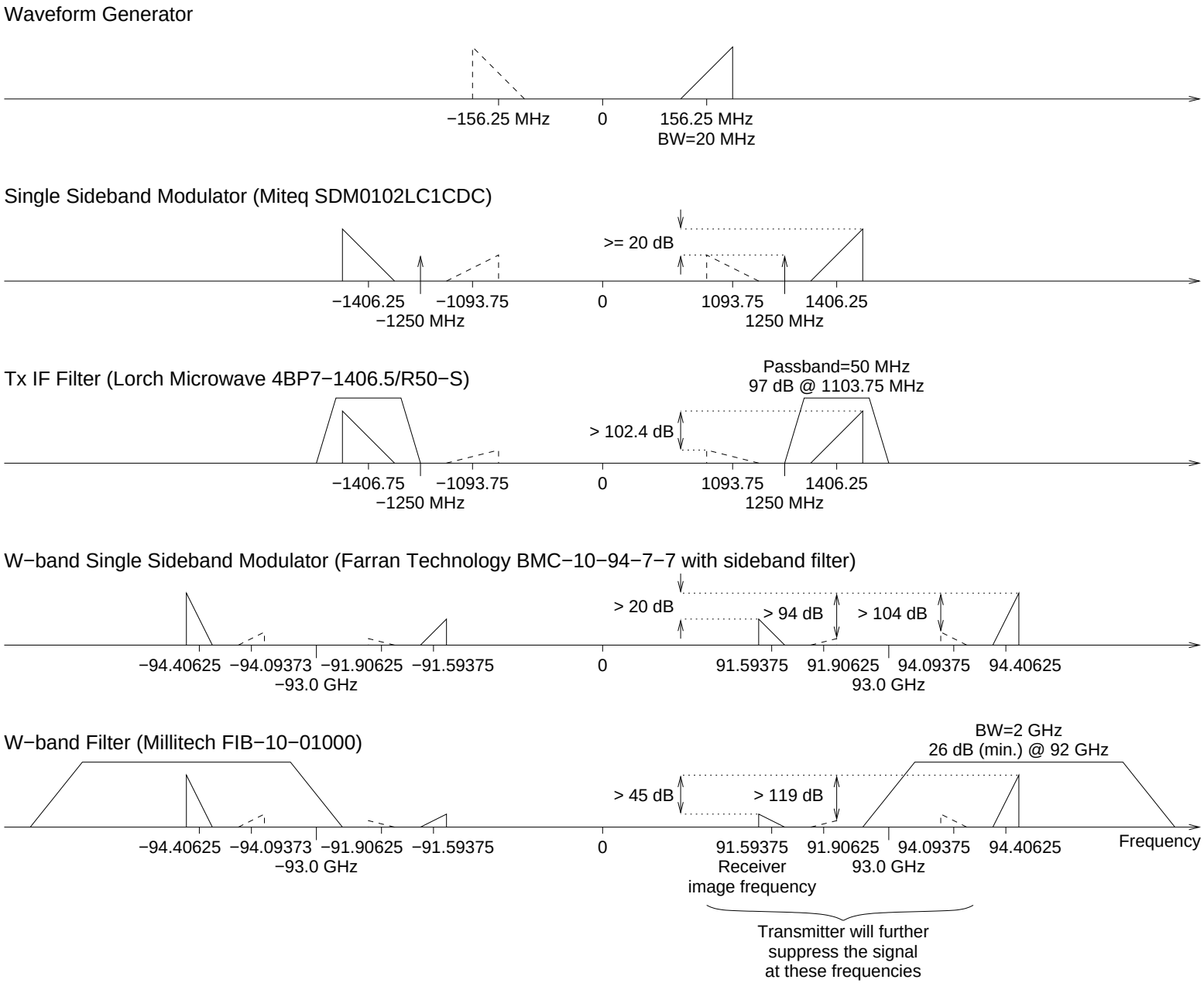

Figure 5: Output of the source and each filter and mixer stage.

The group delay at 146.25, 156.25, and 166.25 MHz is 79.887, 41.658,166.25 ns. Therefore, the maximum phase distortion due to the group delay through the filters are 12.32, 6.42, 25.64 degrees. This phase change can be compensated for by predistorting the transmitted signal to give good range side lobe performance for pulse compression waveforms.

The 156.25 MHz signal is mixed up to 1406.25 MHz using an local oscillator of 1250 MHz (10×125 MHz). The bandwidth of the transmitted signal is up to 20 MHz (146.25 to 166.25 MHz). All mixer products calculated from the first six harmonics of the intermediate frequency and local oscillator fall outside the intermediate frequency band. The closest mixer product to the second stage intermediate frequency band results from the second harmonic of the local oscillator (2500 MHz) and the sixth harmonic of the intermediate frequency (877.5 to 997.5 MHz) and occurs at 1502.5 to 1622.5 MHz which is 96.25 MHz from the second stage intermediate frequency band.

The second stage intermediate frequency filter must suppress the local oscillator signal (1250 MHz), the lower sideband signal (centered at 1093.75 MHz, see Figure 5), and the eighth order harmonic (1502.5 to 1622.5 MHz). The single sideband modulator (Miteq SDM0102LC1CDC) will provide typically 20 dB suppression of the lower sideband, and typically 30 dB suppression of the local oscillator. The local oscillator signal is 156.25 MHz from the desired signal and will not mix back into the receiver band, but the image signal will. Therefore, to achieve 70 dB suppression of the image signal, the filter must suppress the image (1083.75 to 1103.75 MHz) by a minimum of 50 dB. The Lorch Microwave discrete filter, 4BP7-1406.25/R50-S provides 96.7 dB suppression at the image frequencies. The local oscillator signal will be suppressed by 67 dB with this filter. Therefore, the second-stage intermediate frequency image band will be suppressed by greater than 102.4 dB. The eighth order harmonic will be suppressed by a minimum of 28.3 dB with this filter. The group delay at 1381.25,1406.25, 1431.25 MHz is 21.46, 15.6, 19.6 ns. The corresponding phase distortion is 3.3, 2.4, and 3.0 degree.

The signal is mixed up to 94.40625 GHz using a local oscillator of 93 GHz (744×125 MHz). All mixer products that result from the first six harmonics of the second stage intermediate frequency and the local oscillator lie outside the band of interest.

The 94.40625 GHz filter must suppress the 93 GHz local oscillator signal and the image band (91.58375 to 91.91625 GHz, see Figure 5). The W-band single-sideband modulator (Farran Technology BMC-10-94-7-7 with side band filter) will suppress the local oscillator and lower sideband by a minimum of 20 dB. The W-band pass filter (Millitech FIB-10-01000) has a minimum suppression of 25 dB at 93 and 95 GHz. Therefore, the image band will be suppressed by a total of more than 45 dB (see Figure 5). Signals outside the transmitter bandwidth will be further suppressed on transmission.

4.2 Component Impedance Matching

Although Millitech claims that the W-band filter (FIB-10-01000) can be operated with any source and load VSWR, other filter manufacturer vendors recommend that the maximum load VSWR be less than 1.5:1. Because the input VSWR of the EIKA driver amplifier (Farran Technology FPA-10-16-19) is expected to be not better than 2.0:1, an isolator (Millitech JFD-10-RI1SP) is used to improve the VSWR of load seen by the filter.

The extended interaction klystron amplifier (EIKA) input VSWR can be as high as 10.0:1. The maximum load VSWR recommended for the driver amplifier is 2.0:1, so another isolator is used between the driver amplifier and the EIKA.

The EIKA load VSWR must be less than 1.2:1 to achieve the specified performance from the klystron. The directional coupler (Quinstar Technology QJR-W40300) at the output of the EIKA has an maximum VSWR of 1.1:1 which is sufficient to ensure good performance the EIKA. The directional coupler also provides 70 dB of isolation between the klystron and the antenna.

4.3 Power Levels

The nominal output power for the up-conversion electronics is 62 dBm (1600 W). Due to imperfect matching between components, the output power cannot be completely predicted because the input impedance seen by a previous stage depends on the electrical distance between it and the next component. Without simulation tools such as ADS, an accurate estimate of the output power cannot be computed.

The output power analysis was computed using an output power from the driver amplifier of 7.8 dBm which is 2.2 dB below the minimum specified 1 dB compression point of the amplifier. After the isolator, this power level is 7.0 dBm (5 mW). The EIKA typical drive power is +3 to +7 dBm (2 to 5 mW) and has an absolute maximum input power of +10 dBm. Therefore, a 1 dB compression point of the driver amplifier (+10 dBm) is sufficient to drive the amplifier, and provides some degree of protection from over driving the EIKA.

The EIKA can operate with a load VSWR up to 2.0:1 without damage. Therefore, the maximum reflected power for 1.7 kW output power is 190 W. The directional coupler (Quinstar Technology QJR-W40300) provides 30 dB of isolation between the antenna and the transmitter, so that if the antenna were to transmit into a 0 dB return loss load, the transmitter would see a maximum of 1.7 W reflected from the antenna through the directional coupler. If the directional coupler were to fail, the transmitter may be damaged. However, since this design is for a ground-based system, care can be taken to only operate the radar in situations where the reflection from the antenna is not strong (for instance, the antenna will not be pointed towards a solid metal plate).

5 Down-conversion Electronics

The down-conversion electronics in the transceiver are configured as a super-heterodyne receiver. Figure 6 shows a frequency domain representation of the signals implemented in the receiver. Received signals at W-band (94.40625 GHz) are filtered to suppress signals and noise in the receiver image band and then down-converted by a double sideband mixer to an intermediate frequency of 1.406 GHz. The 1.406 GHz IF signal will then be filtered and down-converted to the final IF of 156.25 MHz. This IF signal will pass through a 20 MHz bandwidth anti-aliasing filter before being sampled by the analog to digital converter.

5.1 Spectrum Analysis

Reflections from signals transmitted in the image band of the radar (91.58375 to 91.60375 GHz) are suppressed by the W-band band pass filter in the front-end electronics of the receiver. This filter is the same model and has the same specifications as the filter used in the up-conversion electronics (Millitech

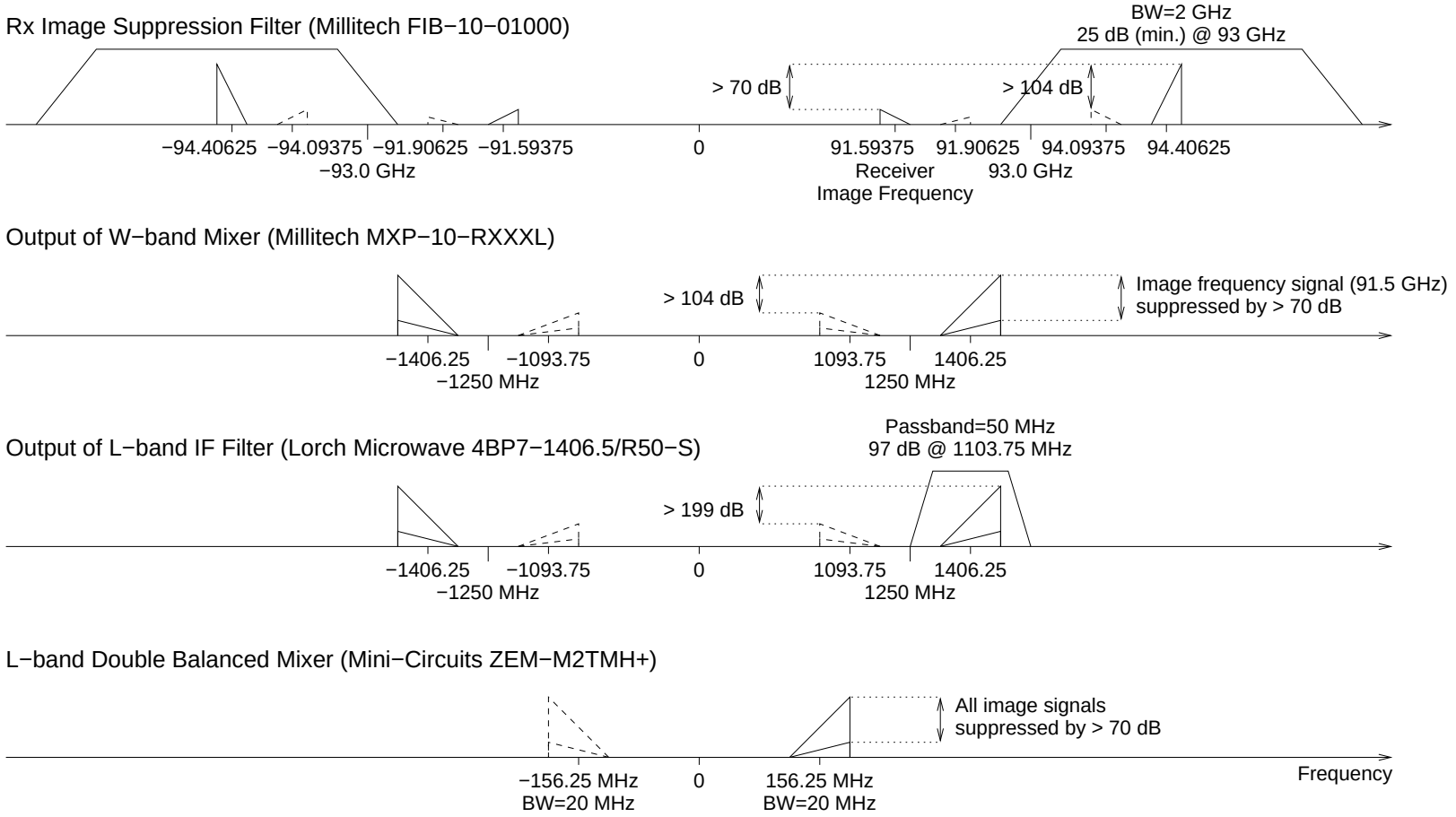

Figure 6: Output of the source and each filter and mixer stage.

FIB-10-01000, 25 dB suppression at 93 GHz). After this filter, the signal in the image band will be greater than 70 dB below the signal at 94.40625 GHz.

The received signal is mixed down from 94.40625 GHz using a local oscillator of 93 GHz (744×125 MHz). All mixer products that result from the first six harmonics of the second stage intermediate frequency and the local oscillator lie outside the intermediate frequency band (1396.25 to 1416.25 MHz). The mixing is performed by a double sideband mixer (Millitech MXP-10-RXXXL). This stage sets the limit on the image-free dynamic range, because the image frequency at 91.59375 GHz mixes to the second stage intermediate frequency. Figure 6 shows that the image-free dynamic range will be greater than 70 dB. The actual image-free dynamic range will probably be much greater than this number, because this number was computed assuming a the W-band filters in the up- and down-conversion electronics suppress the energy in this band by only 25 dB. Since this is the suppression that is achieved at 93 GHz, larger suppression is to be expected over the image band (91.58375 to 91.60375 GHz).

The signal at the second-stage intermediate frequency (1406.25 MHz) is then filtered using a Lorch Microwave 4BP7-1406.25/R50-S cavity filter which suppresses signals in the image band by 97 dB. Signals in the image band at this stage will be greater than 199 dB lower than the signal in the intermediate frequency band, and therefore a double-sideband mixer will be sufficient to down convert the signal to the first stage intermediate frequency (156.25 MHz).

The second stage intermediate frequency signals (1396.25 to 1416.25 MHz) will be mixed down to 156.25 MHz using an local oscillator of 1250 MHz (10 × 125 MHz). All mixer products calculated from the first six harmonics of the intermediate frequency and local oscillator fall outside the first stage intermediate frequency band (146.25 to 166.25 MHz). The closest mixer product to the first stage intermediate frequency band results from the sixth harmonic of the local oscillator (7500 MHz) and the fifth harmonic of the received frequency (6981.25 to 7081.25 MHz) and occurs at 418.75 to 518.25 MHz which is a minimum of 252.5 MHz from the first stage intermediate frequency band, and therefore easy to suppress.

A Mini-Circuits ZEM-M2TMH+ double balanced mixer is used to down convert the signal at 1406 MHz to the first stage intermediate frequency. The first stage intermediate filter (Lorch Microwave 4BP3-156.25/R20-S) is an anti-aliasing filter that conditions the signal for digitization. The signal will be sampled at a rate of 125 MS/s, so the filter suppresses any signals in the range from in the image band (83.75 to 103.75 MHz) by a minimum of 34 dB.

5.2 Component Impedance Matching

As is done in the up-conversion electronics, an isolator (Millitech JFD-10-RI1SP) is used between the filter (Millitech FIB-10-01000) and the Farran FPA-10-16-19 amplifier to provide a better match.

The maximum load VSWR that can be seen by the FPA-10-16-19 amplifier is 2.0:1. The input VSWR of the RF port of the MXP-10-RXXXL is specified to be less than 2.0:1, so not matching component is used between these devices.

5.3 Phase Noise

Phase noise requirements for the 94 GHz stable local oscillator (STALO) are determined by velocity accuracy specification. The transmitted and received signals are up- and down-converted using the same

STALO. Phase noise causes the STALO to decorrelate in the time between transmission of the pulse and reception of reflections from a feature. Oscillator phase noise at Allen variance lags that are smaller than the round trip time (i.e. large offset frequencies from the carrier) contribute more to the decorrelation of the received signal. Thus to calculate the variance in the velocity measurement due to phase noise of the STALO, the integrated phase noise (phase variance) of the oscillator is calculated by integrating a delay dependent phase noise spectrum.

The top plot in Figure 7 shows the phase noise of a W-band STALO, and the bottom plot shows the delay-dependent phase noise spectrum used to calculate the integrated phase noise of the system. For this phase noise spectrum, the integrated phase noise or phase variance for a scatterer 15 km from the radar is 1.5 degrees, which translates to a velocity variance of 0.07 m/s. This is negligible compared to the uncertainty due to aircraft motion (tenths of a meter per second), and therefore will contribute little to the velocity error.

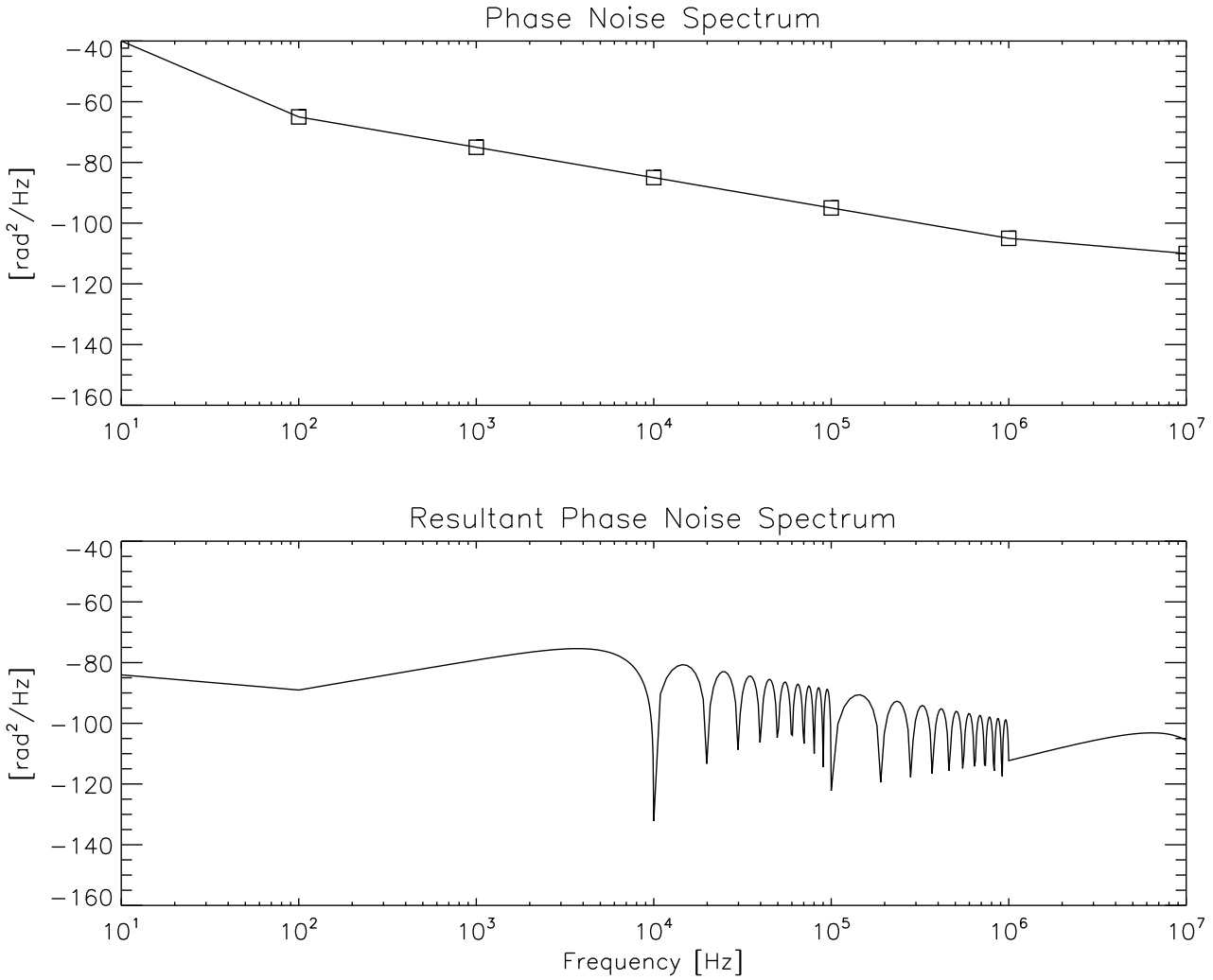

Figure 7: The top figure shows the phase noise spectrum of the 93 GHz local oscillator. The bottom figure shows the phase noise spectrum contribution to the IF signal.

5.4 Dynamic Range

The predicted equivalent noise temperature of the receiver is calculated from

$$(T_e)_N = (T_e)_1 + \sum_{i=2}^{N} \left\{ \frac{(T_e)_i}{\prod_{j=2}^{i} G_{j-1}} \right\} , \tag{1}$$

where $(T_e)_i$ and G_i are the noise temperature and gain of each component in the receiver. The noise figure is then computed from the noise temperature using $(\mathrm{NF})_{\mathrm{dB}} = 10 \log(T_e/T_0 - 1)$. The noise figure of the receiver is 9.3 dB which results in a noise power of −106.5 dBm referenced to the input to the receiver (output of the antenna port) in a 700 kHz bandwidth. This sets the lower end of the receiver dynamic range, and the minimum detectable signal by the receiver.

The upper limit of the receiver dynamic range is set by the maximum input signal to the receiver which is −41.0 dBm. Therefore the receiver dynamic range is 65.5 dB. ADC quantization noise floor is usually set around 10 dB below the receiver noise floor which means that a 14 bit ADC with a dynamic range of around 84 dB will be sufficient for the radar.

The gain of the receiver is determined such that the receiver noise power at the input to the ADC is at least 10 dB higher than the ADC quantization noise power. For an input level of 9 dBm at a frequency of 156.25 MHz and a sampling rate of 125 MS/s, the signal to noise ratio of the sampled signal is listed as 71.2 dB in the LTC2255 data sheet. The quantization noise power referenced to input of the ADC is therefore $9 - 71.2 = -62.2$ dBm, therefore the input noise power must be greater than or equal to −52.2 dBm. For this design, the noise power in the 20 MHz band at the input to the digitizer is −52 dBm. The minimum receiver gain required is 40.0 dB.

6 Calibration

Calibration of the radar requires accurate measurements of the transmitted power, the receiver gain and noise figure. Two methodologies are used to monitor and calibrate the radar: transmitted waveform sampling and noise source calibration.

6.1 Transmit Power

In order to closely monitor the characteristics of the transmitted pulse, a second receive channel is used as transmitted pulse sampling channel. The second receive channel in the system is attached to the directional coupler (Quinstar Technology QJR-W40300) after the EIKA. This channel exists to characterize the magnitude and phase fluctuations that exist in the transmitted pulse. These fluctuations are caused by imperfect regulation of the high voltage pulse in the transmitter, and variations in operating temperature of the klystron.

A sample of the transmitted signal is coupled through the directional coupler to a 30 dB waveguide attenuator. The signal is down-converted and conditioned in the manner as signals in the receiver channel, except that attenuator values have been changed so that the signal level at the digitizer is around -10.66 dBm. The signal to noise ratio for this channel at the input to the digitizer is 41 dB which

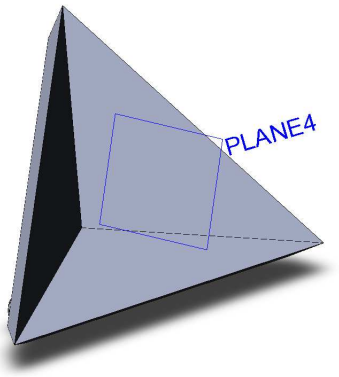

Figure 8: Radar calibration target: trihedral corner reflector

is sufficient for a good characterization of the amplitude and phase characteristics of the transmitted pulse.

6.2 Receiver

The waveguide switch (Quinstar QWZ-WT15) before the low noise amplifier in the receiver can switch between the receive antenna and a noise source. The switch will provide a mechanism to measure the receiver noise figure using the Y-factor method. The sky will provide the cold source and the noise source will provide the hot source. Noise sources with an excess noise ratio of 20.84 dB exist at W-band. These noise sources will provide a noise power of -86 dBm at 273 K and in a 700 kHz band. Using the noise source, The noise figure of the receiver is determined to be 8.9 dB.

6.3 Corner Reflector

A variety of calibration targets such as flat rectangular plate, dihedral corner reflector, metal sphere and trihedral corner reflector, can be used for radar calibration. For HCR calibration, a trihedral corner reflector was chosen for suitable radar cross section.

A diagram of a trihedral corner reflector is shown in Figure 8 [6]. The maximum radar cross-section along the axis of symmetry is

$$\sigma_{max} = \frac{4\pi}{\lambda^2} A_{eff}^2 \tag{2}$$

A_{eff} is the effective area of the trihedral corner reflector. The geometrical relation with the effective area is derived as

$$l = \sqrt{\frac{A_{eff}}{0.289}} \tag{3}$$

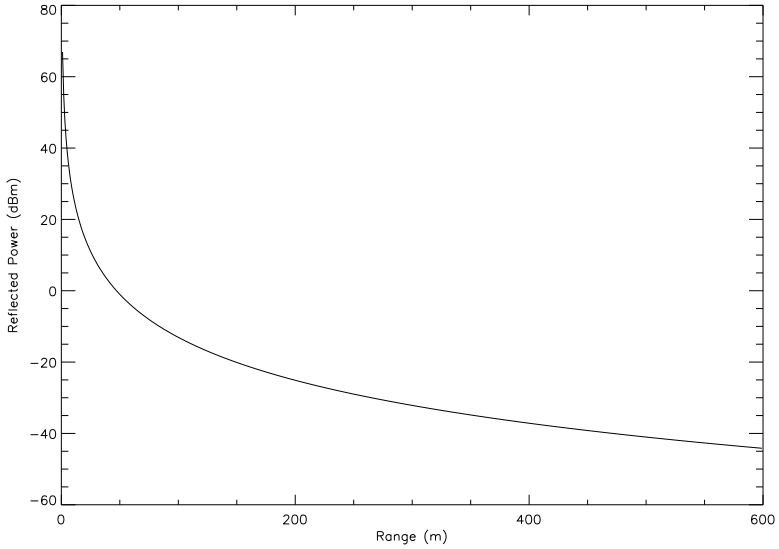

Figure 9: Power reflected from HCR trihedral corner reflector versus range.

where l is the length of each edge of the corner reflector aperture. The 3 dB beamwidth of the radar cross-section σ of the trihedral corner reflector is about 30°. For HCR calibration, we choose l to be 2.375 inch, corresponded to maximum radar cross-section 1.37 m^2. Figure 9 demonstrates the receive power level referenced to input of the LNA.

6.4 System Calibration

A trihedral corner reflector calibration was performed outside NCAR foothills campus. Due to the difficulty in implementing the corner reflector in longer range, the corner reflector is located 100 m from HCR, as shown in Figure 10. A reflector panel is deployed to deflect antenna main beam horizontally in different elevation angles. The elevation angle is set to 1.4° in this setup to minimize ground-clutter interference. The HCR corner reflector is clamped on an adjustable fiberglass flagpole with an industrial-grade tripod base. The height of the flagpole can be adjusted between 3 m to 7.5 m. For a 0.3 m antenna, calibration targets only need to be 60 m away to be in the far-field region. The HCR corner reflector is designed for minimum range of 100 m to avoid receiver saturation. Received power level reflected from a known radar cross-section can be obtained using Equation 4. The expected received power is -12.3 dBm for 100 m range.

$$P_r = \frac{P_t G A_e \sigma}{(4\pi)^2 R^4} \tag{4}$$

To perform HCR calibration, the corner reflector assembly was first offset in azimuthal direction to ensure a position for maximum reflection at the initial height (4.67m). Total height of the assembly is then adjusted in 6-inch increments (15.24 cm). Multiple points in height were recorded for several purposes: to locate maximum reflection height; to investigate the effect of multi-path reflections and to observe the performance of the transmit antenna. Figure 11 demonstrates result of the calibration. The

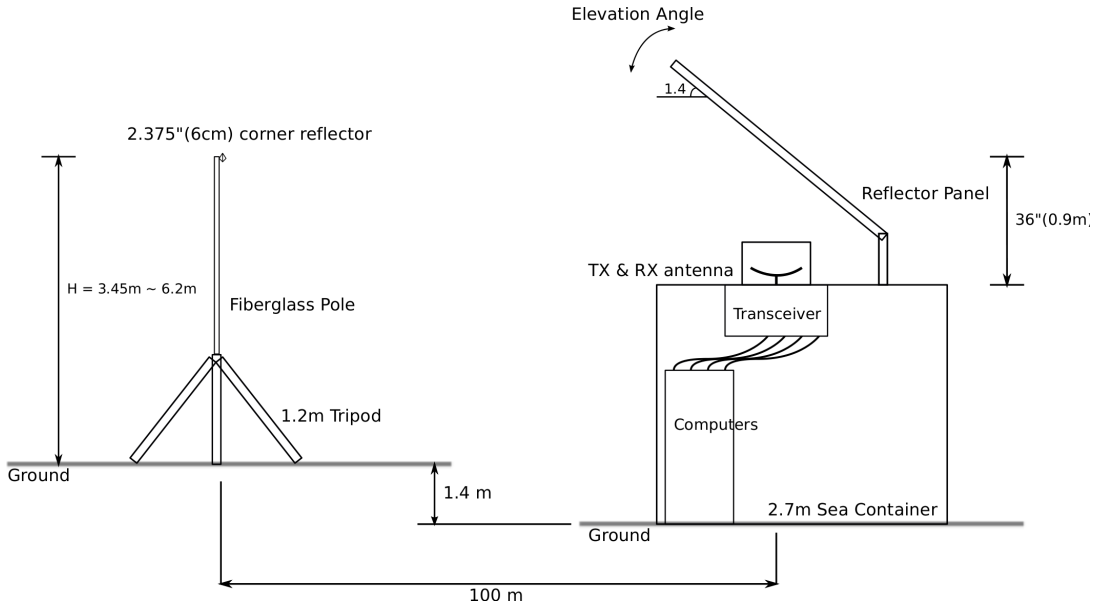

Figure 10: Trihedral corner reflector calibration setup. Calibration target is set at 100 m range due to the difficulty of implementing it at longer range.

received power referenced to input of the LNA is versus corner reflector height is plotted. Maximum power recorded is -20.13 dBm at the height 5.3 m. The power variation is within 1 dB within 1 meter height. This suggests the multi-path reflections are negligible. The -3 dB antenna beam pattern can also be indicated from the measurement. The corresponding height to the -3 dB points is 1.23 m. This indicates the HCR corner reflector was located at the center of the antenna main lobe and also confirms the 3 dB beamwidth of the transmit antenna is about 0.68°. The multi-path reflections appears to be more visible in lower heights. Stronger reflected power at 3.5 m can be due to multi-path reflection.

Note that there is a significant discrepancy (about 8 dB) between the calibration result and the theoretical calculation obtained by Equation 4. This can be due to the antenna parallax. Parallax is significant when high-gain, narrow-beam antenna are used. It is sensitive to relative antenna alignment [5]. Sekelsky and Clothiaux indicate parallax can underestimate radar reflectivity in close range. The bias can be as large as -12 dB with θ_{3dB} angular offset. The theoretical calculation in is based on a single-antenna system which does not encounter antenna parallax uncertainty.

7 System Performance

For the results presented in this section, the antenna diameter is 0.29 m, peak transmitted power is 1125 W, the range resolution is 75 m (500 ns pulse length, 1.4 MHz receiver bandwidth), the pulse repetition frequency is 9.765 kHz, the receiver noise figure is 8.9 dB, the dwell time is 100 ms, the radar is on the ground and stationary, and the radar beam is pointed vertically.

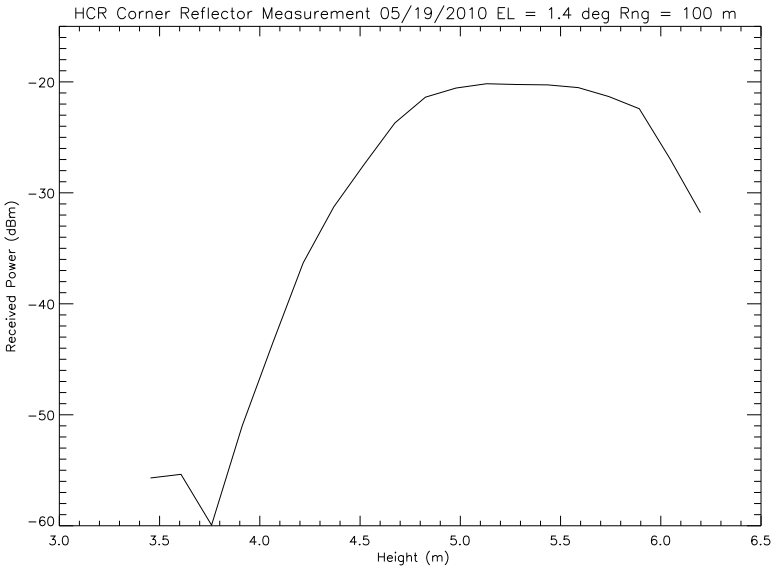

Figure 11: Results of HCR trihedral corner reflector calibration. Received power referenced at input of the LNA versus corner reflector height is shown above.

7.1 Sensitivity and Accuracy

The minimum measurable reflectivity (MMZ) under the conditions of Rayleigh scattering and given as a function of range from the radar is calculated from

$$Z = 10^{18} \frac{2^{10} \log(2) \lambda^2 l_r}{\pi^3 P_t G_a^2 c \tau {\theta_b}^2 \left|K_w\right|^2} P_n R^2 \mathrm{SNR}_{\min} \tag{5}$$

where λ is the wavelength, l_r is the loss due to the finite bandwidth of the receiver, P_t is the transmitted (radiated) power, G_a is the antenna gain, c is the speed of light, τ is the pulse length, θ_b is the antenna beam width, $\left|K_w\right|^2$ is the related to the refractive index of water, P_n is the system noise power, R is the range from the radar, and $\mathrm{SNR}_{\min}$ is defined as the signal to noise ratio such that the reflectivity accuracy ΔZ_{dB} is less than 1 dB. The reflectivity accuracy is calculated from [1, 2]

$$\Delta Z_{\mathrm{dB}} = \frac{4.343}{\sqrt{MN}} \left(\frac{\lambda}{4\pi^{(1/2)} \sigma_w \tau_s} + \frac{1}{\mathrm{SNR}^2} + \frac{2}{\mathrm{SNR}} \right)^{(1/2)} \tag{6}$$

where where M is the number of pulse repetition intervals in the dwell time, N is number of ranges gates averaged, SNR is the linear signal to noise ratio, τ_s is the pulse repetition time, σ_w is the spectral width of the scatterers. Using Equation 6, we can calculate the signal to noise ratio that is required for a 1 dB reflectivity accuracy. Table 3 shows that at a signal to noise ratio of -7.8 dB, the reflectivity accuracy is 1 dB (these values are highlighted in bold font in the table).

The minimum measurable reflectivity is calculated for the atmospheric conditions described by a mid-latitude summer profile of pressure, temperature and water vapor density (top three panels of Figure 12). The atmospheric attenuation due to oxygen and water vapor is then calculated using the Millimeter-wave Propagation Model (MPM93, [3]) as a function of height from the profile data (lower left-hand

Table 3: Standard deviation in reflectivity measurement (dB).

	Spectral Width (m s^{-1})				
SNR (dB)	0.25	0.5	1	1.5	2
−7.8	1.11	1.04	**1.00**	0.98	0.98
0	0.62	0.47	0.37	0.34	0.31
10	0.57	0.41	0.30	0.25	0.21
20	0.57	0.41	0.29	0.24	0.21
30	0.57	0.41	0.29	0.24	0.21

panel in Figure 12). The attenuation profile is integrated to determine the cumulative attenuation as a function of range (lower middle panel in Figure 12), and the minimum detectable reflectivity (lower right-hand panel in Figure 12) is calculated using Equation 5. Minimum measurable reflectivity for a vertical profile are tabulated for specific ranges in Table 4.

Table 4: Minimum measurable reflectivity as a function of range from the radar.

Range (km)	1	2	5	10
MMZ (vertical profile from 12 km)	−39.6	−33.5	−25.6	−19.6

7.2 System Dynamic Range

The receiver dynamic range (67.7 dB) is less than the system specification value of 80 dB. However, as is shown above, atmospheric reflections with power value less than the noise floor can be measured to a specified accuracy by integration received power measurements. Specifically, the reflectivity can be measured with a 1 dB accuracy for a signal with a signal to noise ratio of -7.8 dB. For the parameters listed above, the system dynamic range is 75.2 dB (this value is 0.3 dB less than $7.8 + 67.7$ dB because the brightness temperature of the background scene add to the noise in the system). While this value still is still less than 80 dB, it is probably the best that can be achieved with commercially available hardware.

8 Observations

8.1 Vertical observation

Vertical profiles of a pre-thunderstorm environment were observed on May 29, 2010. HCR collected nearly hour-long data prior to a thunderstorm. Precipitation was reported around 5:30pm in Boulder area. Figure 13 and 14 demonstrate a sample dataset from the hour-long observation. HCR was operated with 75 m resolution and 9.765 kHz repetition frequency. This configuration results in ±7.75 m/s

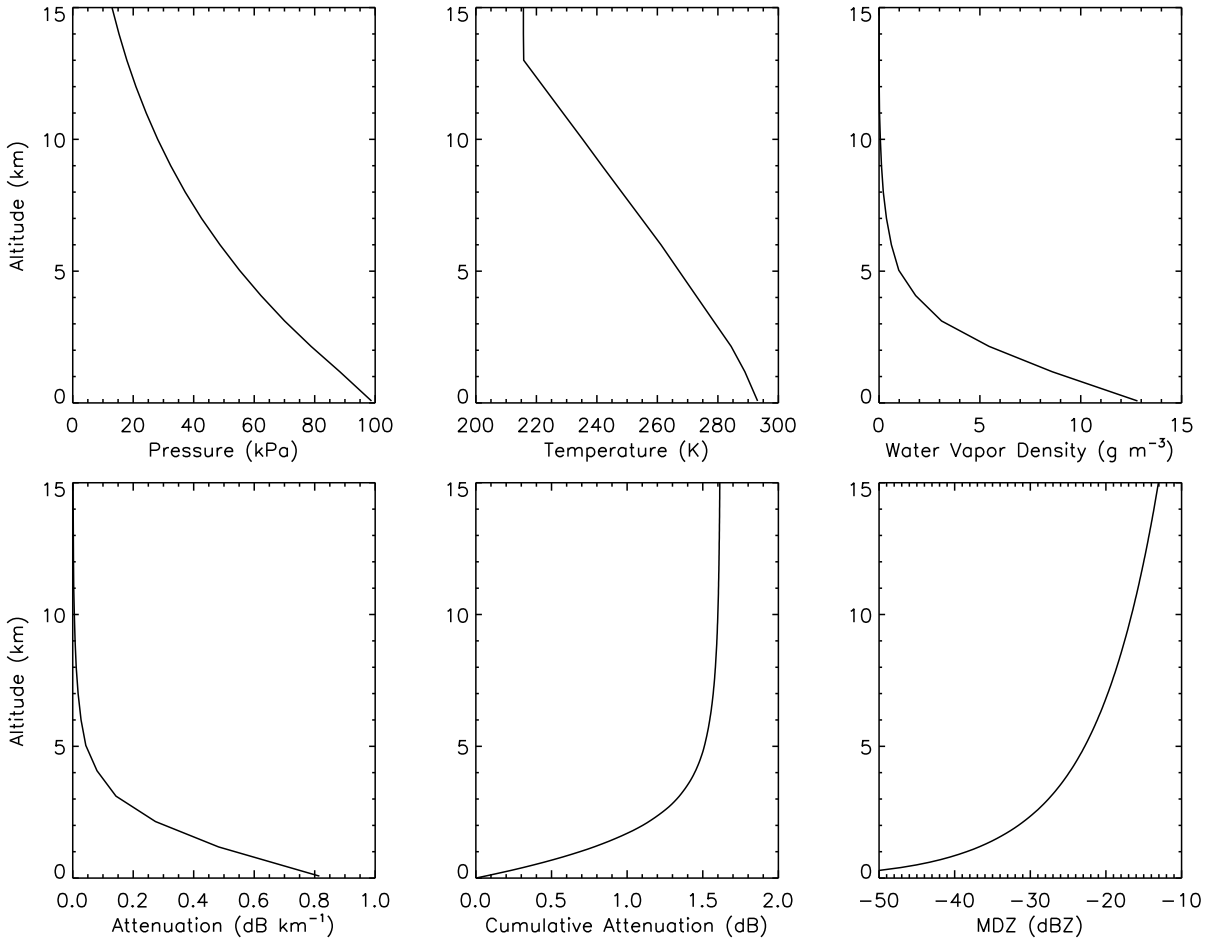

Figure 12: Simulated minimum detectable reflectivity for a vertical profile. The radar is at an altitude of 12 km.

unambiguous velocity. The reflectivity, the upper plot in Figure 13, shows cloud returns as high as 11 dBZ in 5 km range. The radar also resolves echoes -34 dBZ in 1 km range. A noticeable object was observed at 10.2 km height. It may be a commercial jet plane passing through the radar beam volume at its cruising altitude about 33,000 ft. This observation coincides with the velocity calculation – the object does not have vertical velocity component in Figure 13 lower plot. It appears to pass by the radar beam in tangential direction briefly. The velocity calculation suggests the cloud volume has a slow mean velocity 0.48 m/s aloft in 4 to 5.5 km range (red). Clouds transitions from upwards velocity, 0.3 m/s to downwards motion -1.5 m/s (blue) above 5.5 km. Nearly zero mean velocity at the surface suggests there was higher moisture content near ground. Figure 14 represents the spectral width and signal-to-noise ratio of the same dataset. The median spectral width in 3.75 km to 6 km range is 0.368 m/s. This suggests the band of cloud is uniformly distributed with very little turbulence. The echo near surface has, on the other hand, more shear. The corresponding spectral widths range between 2 to 4 m/s. Signal-to-noise ratio in Figure 14 indicates approximately 35 dB SNR in the cloud band. Weak targets are detected by HCR receiver as far as 10 km. The echo from the commercial aircraft at 10 km appears to have 3 dB SNR. This confirms that the bright echo in the upper Figure 13 is still a reliable measurement.

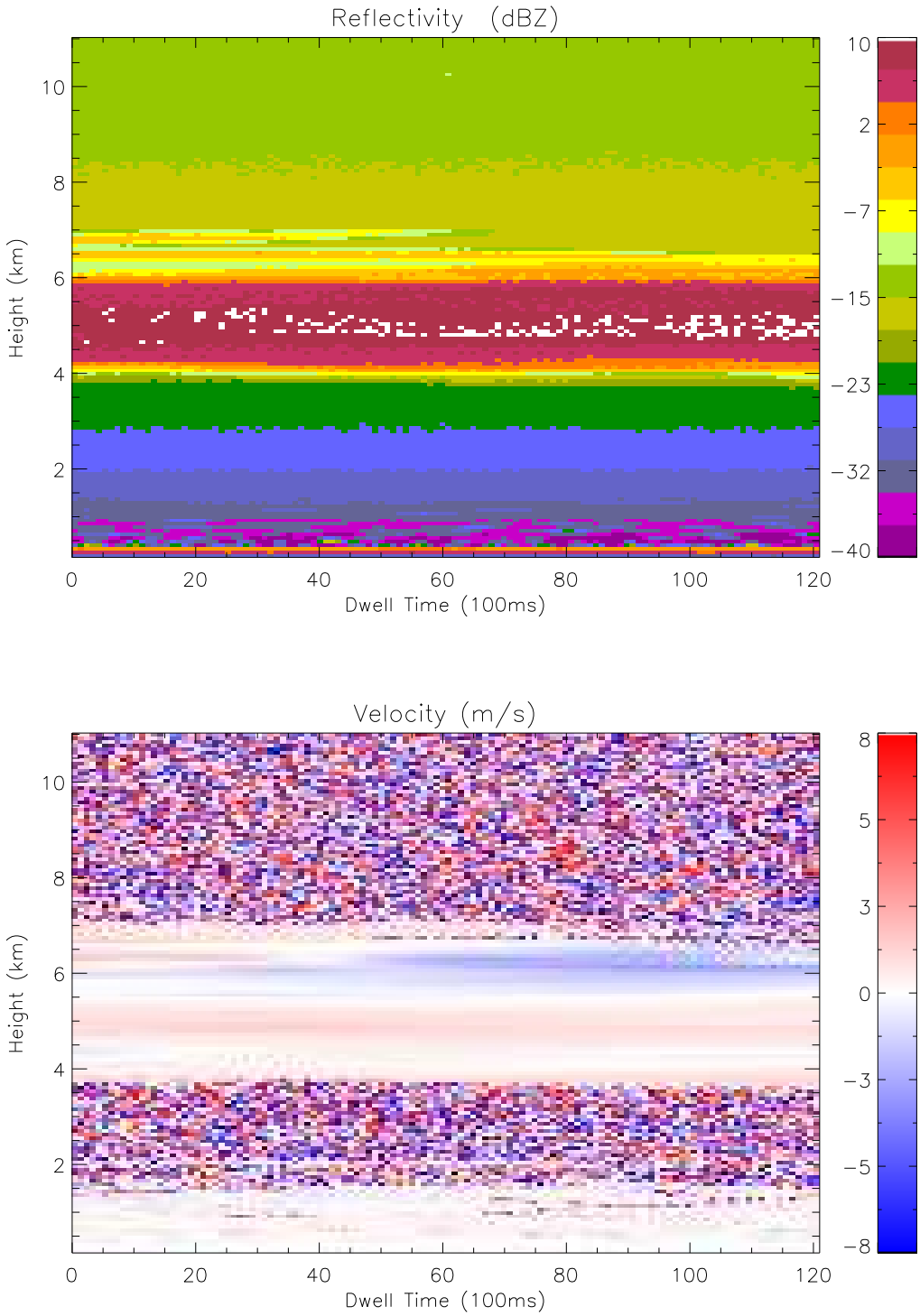

Figure 13: 10 km vertical profiles of a pre-thunderstorm environment. Upper: Reflectivity. A band of clouds were observed around 5 km range. Lower: Velocity. Unambiguous velocity is ± 7.75 m/s. Colored red for upwards motion, blue for downwards velocity. 22:04:58Z on May 29, 2010.

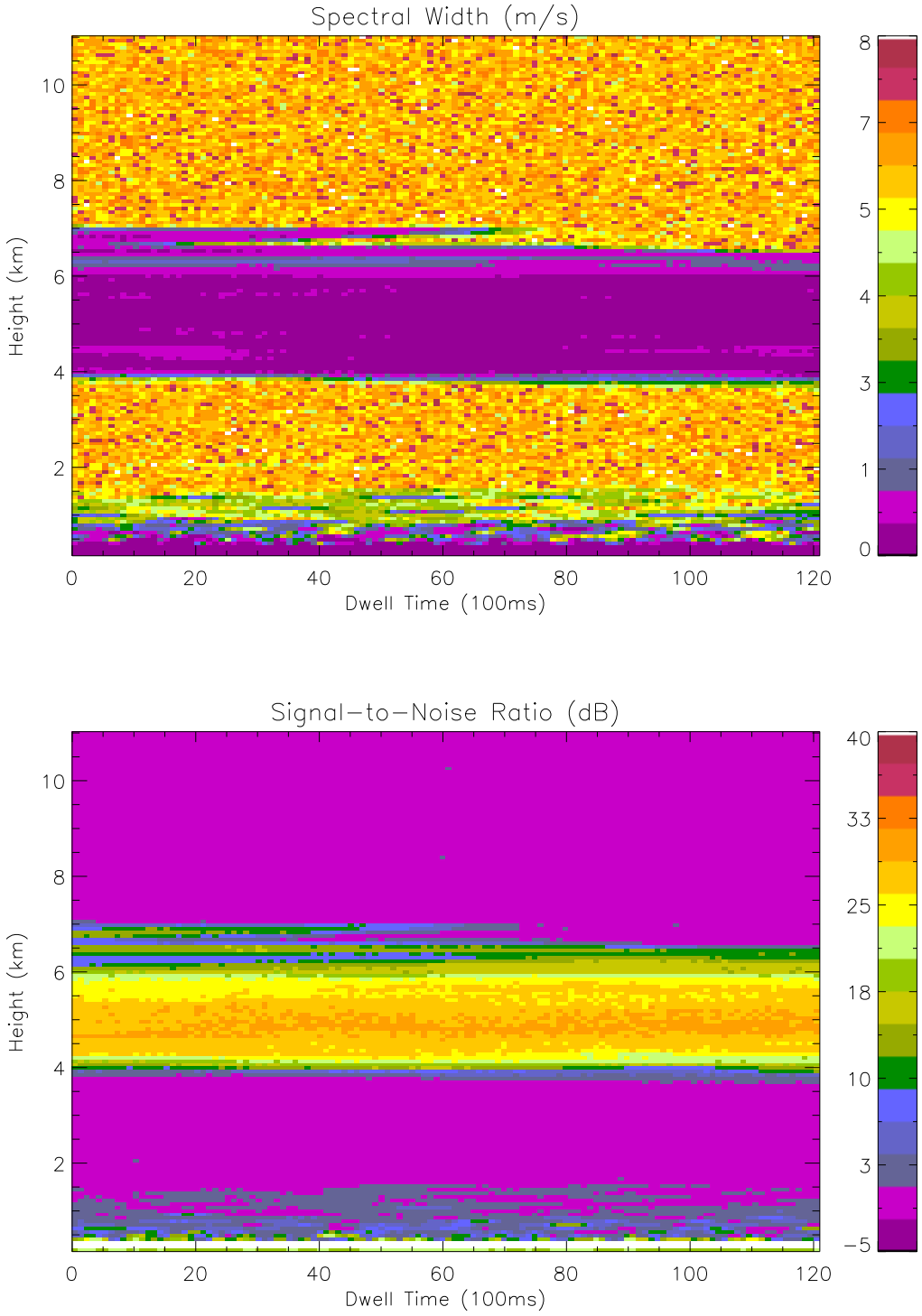

Figure 14: Spectral width (upper) and signal-to-noise ration (lower) of the vertical profile 22:04:58Z on May 29, 2010. The commercial aircraft echo at 10 km height still has a 3-dB SNR.

8.2 NexRad Comparison

In order to compare measurements from HCR with the nearby NexRad(KFTG), the characteristic dimension of the hydrometeors needs to be small compared to the wavelengths of both radars. This criteria ensures the scattering mechanism to be in the Rayleigh region. The radar cross-section in the Rayleigh region is proportional to the fourth power of the frequency, and is determined more by the volume of the scatterer than by its shape [7]. For a preliminary comparison between a S-band and a W-band radar, the scatterer dimension is needed to be small. HCR collected some vertical profiles while the NexRad was operated in clear-air mode on June 1, 2010. The estimated beamwidth of the KFTG over foothills lab is about 1.1 km and the height of beam center is 3.83 km. Figure 15 demonstrates the KFTG reflectivity in Boulder area. The time stamp indicates the starting time of the volume scan. Since there are several tilts in every scan, the starting time of the appropriate PPI scan over foothills lab was interpolated. The corresponding HCR vertical profile is shown in Figure 16. A band of strong echo appears at 4 km height and has average reflectivity of 12.27 dBZ. A uniformly upwards velocity 0.95 m/s is shown in the lower Figure (colored red). The corresponding median spectral width is 0.401 m/s. The velocity and spectral width measurements suggest a band of small-sized, uniformly distributed, non-turbulent droplets are suspended in the air. This may be in agreement with our assumption that both radar are in the Rayleigh scattering region.

An equivalent 1.1 km vertical observation volume was integrated in HCR data for comparison. To simulate the antenna beam characteristics, a Gaussian weighing function was applied to the integrated volume. The volume is centered at 4.125 km AGL, and has the height of 1.1 km. The corresponding vertical 3-dB beamwidth is 43 m at the bottom and 55 m at the top of the volume. The integrated, Gaussian weighted reflectivity of the vertical observation volume versus dwell time is plotted in Figure 17. The integrated reflectivity varies from 7 dBZ to 3 dBZ within 12 seconds period.

Despite the minor issues in the observation volume matching, data time alignment and height discrepancy, this preliminary comparison indicates that HCR measurements are only a few dB from a calibrated instrument, KFTG.

9 Summary and Future Work

Detailed design considerations, radar calibration, performance assessment and two sample observations are presented in this document. The vertical observation demonstrates the sensitivity of HCR at high altitude and the capability of measuring target velocity. The preliminary performance comparison with nearby NexRad, KFTG demonstrates that HCR ground-based prototype measures close to meaningful, calibrated reflectivity even with the antenna parallax uncertainty.

HCR completed the development in the single polarization, dual-antenna configuration. The characteristics of the transceiver has been documented. Several issues such as antenna parallax and calibration discrepancy need to be further investigated in future HCR configurations.

A tremendous amount of efforts have been put into more in depth design for the single polarization, single-antenna, airborne configuration. Critical components such as millimeter-wave polarization switches, airborne-grade transmitter and the antenna will be delivered in the near future for airborne development.

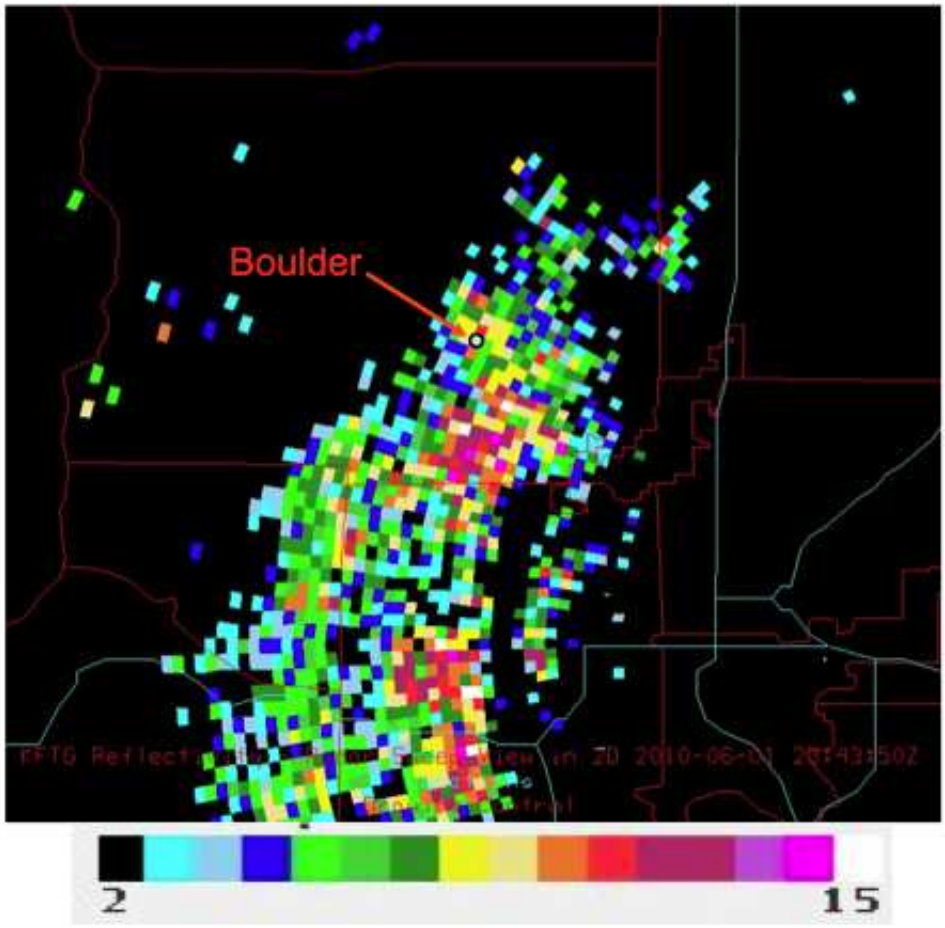

Figure 15: KFTG Reflectivity in Boulder area 23:43:50Z on June 1, 2010. Average of KFTG reflectivity values surrounding Boulder is 8.55 dBZ.

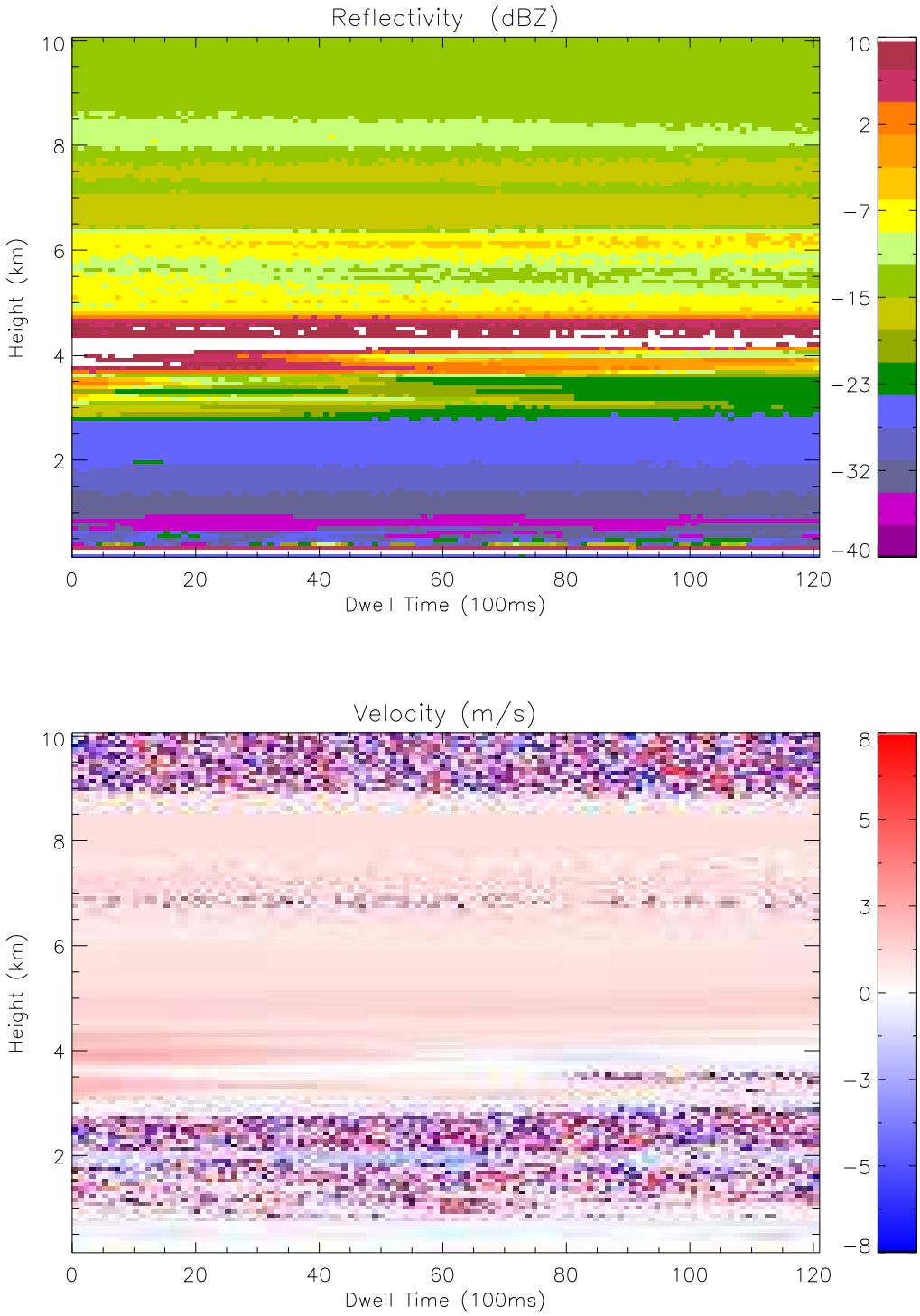

Figure 16: Vertical reflectivity (upper) and velocity (lower) profile at 23:45:07Z , June 1, 2010.

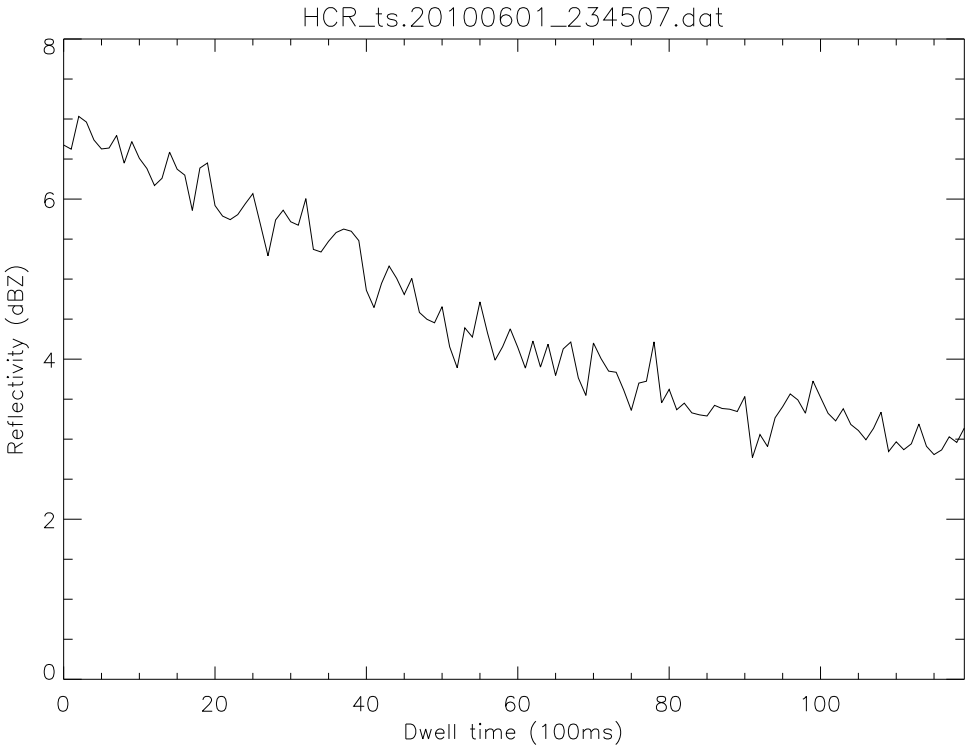

Figure 17: Integrated Gaussian weighted reflectivity of the equivalent observation volume of KFTG 4.125 km AGL versus dwell time.

A Intermediate Frequency

The intermediate frequency and analog to digital sampling rate selected for the radar are 156.25 MHz and 125 MS/s respectively. This section describes the factors that resulted in these selections. Other intermediate frequency and sampling frequency combinations are discussed in Section A after the waveform generator design has been presented.

The HCR will use pulse compression to increase the sensitivity of the system. Since pulse compression waveforms used in radars with range resolutions of tens of meters have bandwidths in the megahertz to tens of megahertz range, the intermediate frequency must be sufficiently high to provide enough bandwidth for sufficient suppression of unwanted harmonics and mixer products. Therefore, intermediate frequencies in the tens to hundreds of megahertz are desirable.

The HCR will be used in an airborne environment in which the VHF aviation communications band (Airband, 108 to 137 MHz) exists. To eliminate interference in the radar signals from aircraft communications, the HCR intermediate frequency must be chosen outside this band. In addition, the intermediate frequency must be high enough to support wide bandwidth (up to 20 MHz) signals, and if possible, when sampled by the digitizer, alias to the frequency that is equal to the sampling frequency divided by four. This latter requirement allows for the implementation of the $f_s/4$ demodulation scheme for narrow-band signals which simplifies the digital demodulation logic. However, the intermediate frequency is limited by the technology available to generate an arbitrary wide bandwidth waveform, and the ability to suppress undesired mixer products that result from the frequency up- and down-conversion process.

An intermediate frequency of 156.25 MHz, in conjunction with a sampling frequency of 125 MS/s, satisfies the $f_s/4$ demodulation scheme for narrow-band signals. A signal centered at 156.25 MHz will alias to 31.25 MHz when sampled at a rate of 125 MS/s, and 31.25 MHz is one quarter of 125 MHz as required.

B Waveform Generator

The advent spread spectrum coding schemes such as CDMA, TDMA, and OFDM in communications has provided a demand for wide-bandwidth high-speed digital to analog converters (DACs) that include digital up-conversion circuitry. These up-converting DACs are ideal for generating pulse compression waveforms with an arbitrary amplitude taper and frequency modulation that allows one to predistort a pulse compression waveform in amplitude and phase to compensate for amplitude and phase distortions due to microwave components in the transceiver. Several vendors have incorporated these DACs into transceiver cards which is appealing because these cards have both a DAC for generating the waveform for transmission, and digital down-conversion (DDC) electronics to digitize received signals. Based on a survey of available cards, the best choice in terms of size and functionality appears to be the Pentek Model 7142 which has a single channel 16-bit 500 MS/s interpolating and up-converting DAC (Texas Instruments DAC5686/7), and four 14-bit 125 MHz analog to digital converters (Linear Technologies LTC2255). The card is in the PMC form factor which can be mounted on various other carrier cards sold by Pentek including CompactPCI.

In addition to the features mentioned above, the Model 7142 is appealing because it is similar to the Model 7140 that the EOL wind profilers will use. Thus, software developed for one system could be

reused in the other. The differences between the cards are that the 7142 provides a Xilinx Virtex-4 FPGA as opposed to GC4016 Gray Chips and a Xilinx Virtex-II FPGA to implement the DDC, and the 7142 only routes one of the two DAC5686/7 analog outputs to a connector on the front panel of the board. This difference means that the DAC5686/7 can only be used in the single channel or quadrature modulation mode, and cannot be used in the single-sideband mode that was originally envisioned in the HCR Preliminary Design Review document.

This section presents simulations that show that the performance of the DAC5687 used on the Pentek Model 7142 is suitable for use in the HIAPER Cloud Radar. Section B.1 provides an introduction to distortions present in the output of DACs. Section B.2 details how the waveform will be synthesized with this device, and the results of simulations of waveforms with the the device.

B.1 Distortions in DAC-Generated Signals

Digital to analog converters do not produce a perfect analog representation of the digital input signal. The output signal is corrupted through the non-linear mapping of the input codes to output codes, and clock-related spurious signals. The effect of these distortions must be understood in the application in which the DAC is used. The theory of digital to analog converters is well documented (e.g. [8]), and thus, this section only provides a brief overview of the distortions considered in this design study.

B.1.1 Harmonic Signals

The output code is a combination of the input code, the integral non-linearity error, the gain error, and the offset error, and is given by

$$O(I) = \left(I + \epsilon^I_{\text{lsb}}\right) \frac{F - \epsilon_{\text{g}}}{F} + \epsilon_{\text{offset}} \tag{7}$$

where I is the input code, $O(I)$ is the output code, ϵ^I_{lsb} is the integral non-linearity error associated with the input code, F is the full scale code, ϵ_{g} is the gain error, and ϵ_{offset} is the offset error. The definition of each of these terms is defined in detail in various texts and will not be repeated here. The values are typically listed in the DAC data sheet.

The non linearity of the conversion from the input code to the output voltage generates harmonics of the output signal. An example spectrum of a DAC signal is shown in Figure 18. In this example, the output signal is centered at a frequency of 25 MHz, and the output sample rate from the DAC is 120 MHz. The top part of the signal shows the result of the non-linear conversion which generates harmonics of the desired output signal at integer multiples of the output signal frequency. The desired output signal is drawn in black, and the first eight harmonics are drawn in various colors and are labeled with their harmonic number. The signals in the negative part of the spectrum are drawn with dashed lines. Since the output waveform is a continuous representation of a sampled process, the harmonics outside the Nyquist zone (−60 to 60 MHz) aliases into the Nyquist zone, and the result is sketched in the bottom part of the figure. In this example, the desired signal is corrupted by the forth and sixth harmonics. In general, the frequency of the aliased harmonics is determined by the frequency of the desired signal and the output DAC sampling rate. The level of the harmonics is determined by the non-linear error in the conversion processes which in general is different for each DAC.

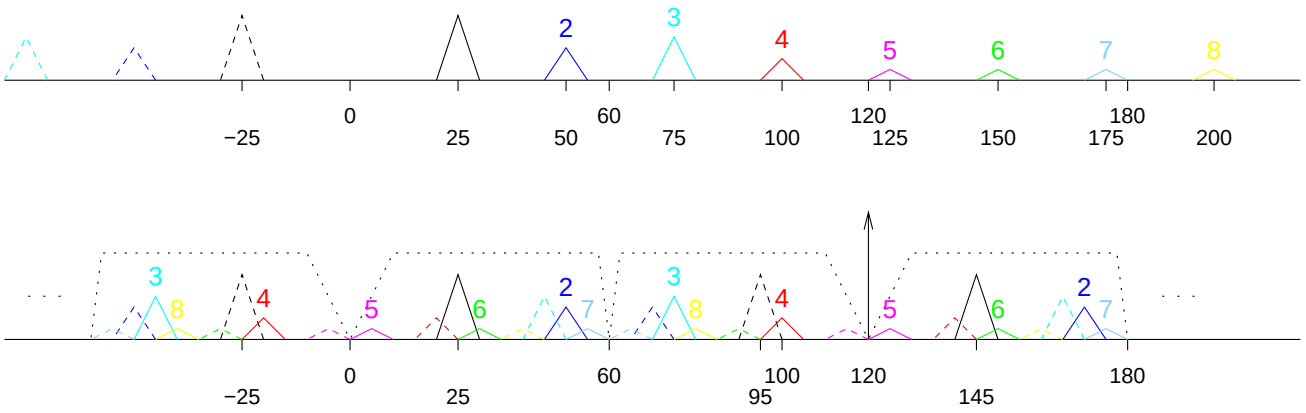

Figure 18: The top part of the figure shows the harmonics of an output signal centered at 25 MHz. The bottom part of the figures shows how these harmonics are mapped into the Nyquist range.

B.1.2 Non-Harmonic Spurious Signals

Many high speed DACs are able to interpolate between input samples to produce an output rate that is higher than the input rate. Typical interpolation factors are 2, 4, 8, and 16. Interpolation provides high output sample rates without the need for an equivalent input sample rate, and separates the desired signal from images in adjacent Nyquist zones. However, the subharmonic frequencies of the DAC clock that are used for the interpolation filters, mix with the DAC clock due to imperfect isolation between the internal digital logic and DAC clock circuits, and create images of the desired signal. The amplitude and location of these spurious signals in the frequency spectrum depend on the frequency of the desired output signal, the DAC output rate, and the amount of interpolation. In many situations, these spurious signals are the dominant signals that exist close to the desired signal frequency, and therefore can be hard to filter.

B.2 Waveform Generator Implementation and Analysis

The intermediate frequency and sampling rate are 156.25 MHz and 125 MS/s respectively. The 156.25 MHz signal will be generated by the DA5687 internal digital up-conversion circuitry. A functional block diagram of the DAC5687 in the `X4L/FMIX/CMIX` mode and with `cm_mode(3:0) <= 1001` (`CONFIG2` register) is shown in Figure 19. The real $I[n]$ and imaginary $Q[n]$ parts of a base band signal are the input to the DAC5687. The input sampling rate is 125 MS/s. These signals are interpolated up to a sampling rate f_{s_1} of 250 MS/s ($I_{\text{x2}}[n]$ and $Q_{\text{x2}}[n]$). The fine mixer stage of the DAC5687 uses an NCO running at 250 MS/s to generate a Hilbert transform pair ($m_{\text{x2}}[n]$ and $m_{\text{x2}h}[n]$) centered at a frequency f_{c_1} of 31.25 MHz at the output of the fine mixer stage (see DAC5687 datasheet, p. 37 in the section on the fine mixer or p. 68).

$$
\begin{aligned}
m_{\text{x2}}[n] &= I_{\text{x2}}[n]\cos\left(2\pi\frac{f_{c_1}}{f_{s_1}}n\right) - Q_{\text{x2}}[n]\sin\left(2\pi\frac{f_{c_1}}{f_{s_1}}n\right) \\
m_{\text{x2}h}[n] &= I_{\text{x2}}[n]\sin\left(2\pi\frac{f_{c_1}}{f_{s_1}}n\right) + Q_{\text{x2}}[n]\cos\left(2\pi\frac{f_{c_1}}{f_{s_1}}n\right)
\end{aligned}
\tag{8}
$$

This Hilbert transform pair of signals is then interpolated to a sampling rate f_{s_2} of 500 MS/s ($m_{\mathrm{x4}}[n]$ and $m_{\mathrm{x4}h}[n]$), and these signals become the input to the course mixing stage. The course mixing stage in the DAC5687 is limited to frequency up-converting signals by either $f_{s_2}/2$ or $f_{s_2}/4$. In this application, the $f_{s_2}/4$ mode is used to frequency up-convert the Hilbert transform pair to single sideband signal centered at 156.25 MHz. The inverse sinc filter ($x/\sin x$) is used to compensate for gain changes across the band due to the zero-order hold output of the DAC. The input to the digital to analog converter (DAC A) in the DAC5687 is

$$y[n] = m_{\mathrm{x4}}[n]\cos\left(2\pi\frac{f_{c_2}}{f_{s_2}}n\right) - m_{\mathrm{x4}h}[n]\sin\left(2\pi\frac{f_{c_2}}{f_{s_2}}n\right) \tag{9}$$

$$= I_{\mathrm{x4}}[n]\cos\left(2\pi\frac{f_{c_1}+f_{c_2}}{f_{s_2}}n\right) - Q_{\mathrm{x4}}[n]\sin\left(2\pi\frac{f_{c_1}+f_{c_2}}{f_{s_2}}n\right) \tag{10}$$

where $f_{c_1} + f_{c_2}$ =156.25 MHz, and f_{s_2} =500 MS/s. This signal is a single sideband signal (upper sideband) centered at 156.25 MHz.

The course mixing stage output sequence is selected by bits `cm_mode(3:0)` in the `CONFIG2` register. With $f_{c_2} = 125$ MHz and $f_{s_2} = 500$ MS/s, Equation 9 simplifies to

$$y[n] = m_{\mathrm{x4}}[n]\cos(2\pi n/4) - m_{\mathrm{x4}h}[n]\sin(2\pi n/4) \tag{11}$$

which, for $n = 0, 1, 2, 3, 4, 5, \ldots$,

$$y[n] = m_{\mathrm{x4}}[0],\ -m_{\mathrm{x4}h}[1],\ -m_{\mathrm{x4}}[2],\ m_{\mathrm{x4}h}[3],\ m_{\mathrm{x4}}[4],\ -m_{\mathrm{x4}h}[5],\ \ldots$$

The course mixing output sequence sequence for this application is found by comparing the sequence above with the sequences found in Table 10 of the DAC5687 datasheet (p. 38). In this case, the sequence corresponds to the sequence associated with the output from DAC A with `cm_mode(3:0) <= 1001`.

This document does not yet describe how to set up the FIR filters in the DAC5687 or any of ther other registers to configure the DAC for the mode of operation discussed.

As described in Section B.1.2, the interpolation provided by the DAC5687 causes non-harmonic spurious signals in the output. Table 5 lists the frequency and worst-case level of these spurious signals. The signals at 93.75 and 218.75 MHz are both 62.5 MHz from 156.25 MHz, and will need to be suppressed by around 30 dB. These signals will define the requirements for the bandpass filter at the output of the DAC.

The closest harmonically related signals generated by the DAC were calculated through a simulation that used the integral non linearity error data provided by Texas Instruments, and the gain and offset error from data sheet for the DAC5687. The simulated output waveform and spectrum of the DAC, without the inverse sinc compensation, is shown in Figure 20. A DC component to the spectrum is predicted due to the offset error of the DAC. Figure 21 shows the same spectrum over a reduced frequency range, and identifies the locations and levels of the first 15 harmonics between 0 to 250 MHz. These harmonics are also tabulated in Table 6. The closest harmonics occur at 31.25 MHz from the intermediate frequency signal at 125 and 187.5 MHz, but are more than 90 dB below the carrier.

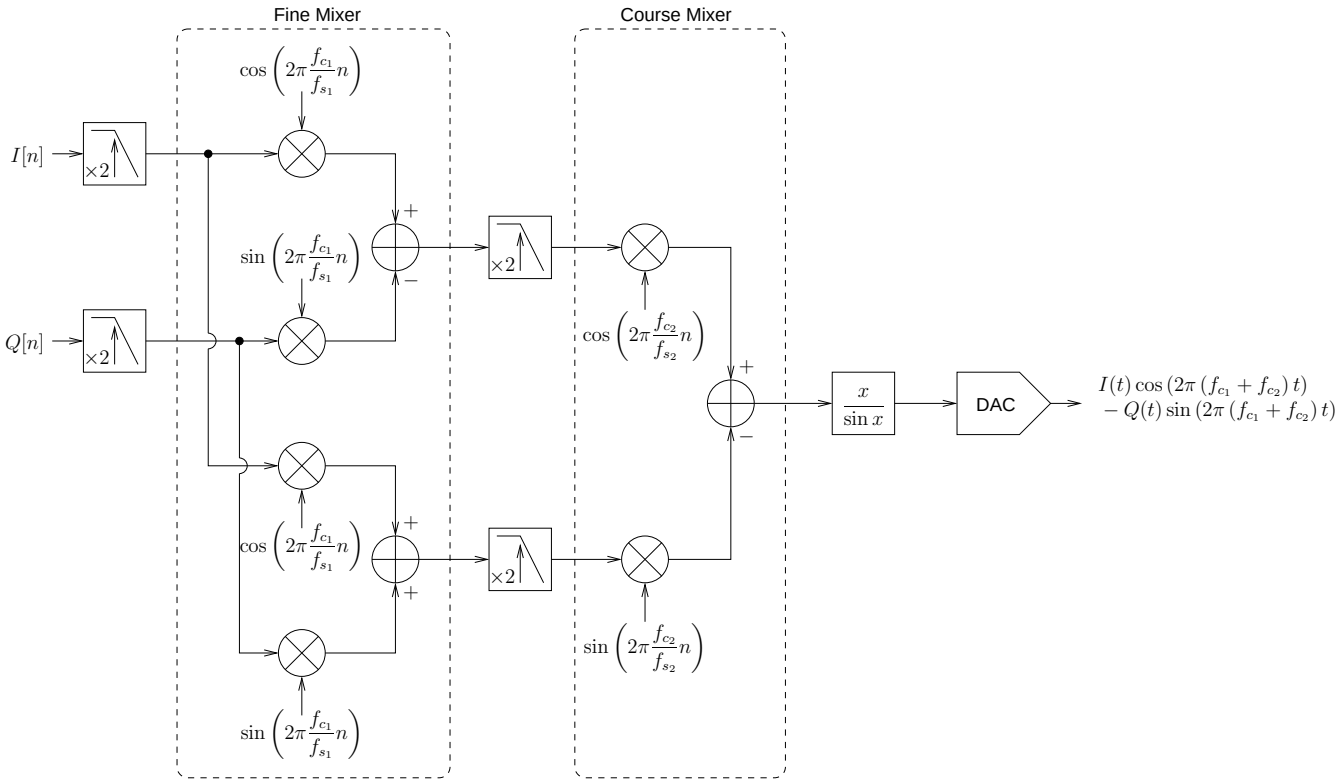

Figure 19: DAC5687 X4L operating mode. In- and quadrature-phase samples are interpolated to twice the input sampling rate, and then frequency up-converted to an intermediate frequency (31.25 MHz) by the fine mixer stage. The result it a Hilbert transform pair which is interpolated by a factor of two again, and then frequency up-converted to the final intermediate frequency (156.25 MHz).

Table 5: DAC spurious output signals due to clock related mixing internal to the DAC.

Spurious	**Frequency**	**Level**
	MHz	dBc
$f_{\text{SIG}} + \frac{f_{\text{DAC}}}{4}$	281.25	−41
$f_{\text{SIG}} - \frac{3}{4}f_{\text{DAC}}$	218.75	−41
$f_{\text{SIG}} - \frac{f_{\text{DAC}}}{2}$	93.75	−47
$f_{\text{SIG}} - \frac{f_{\text{DAC}}}{4}$	31.25	−41

The simulation did not consider clock jitter or the effects of only using a 32-bit NCO in the first stage of the up-conversion. However, if the resolution of the NCO causes the harmonics to increase significantly, the input signal can be changed to the Hilbert transform pair of signals sampled at 125 MS/s and the fine mixer stage bypassed.

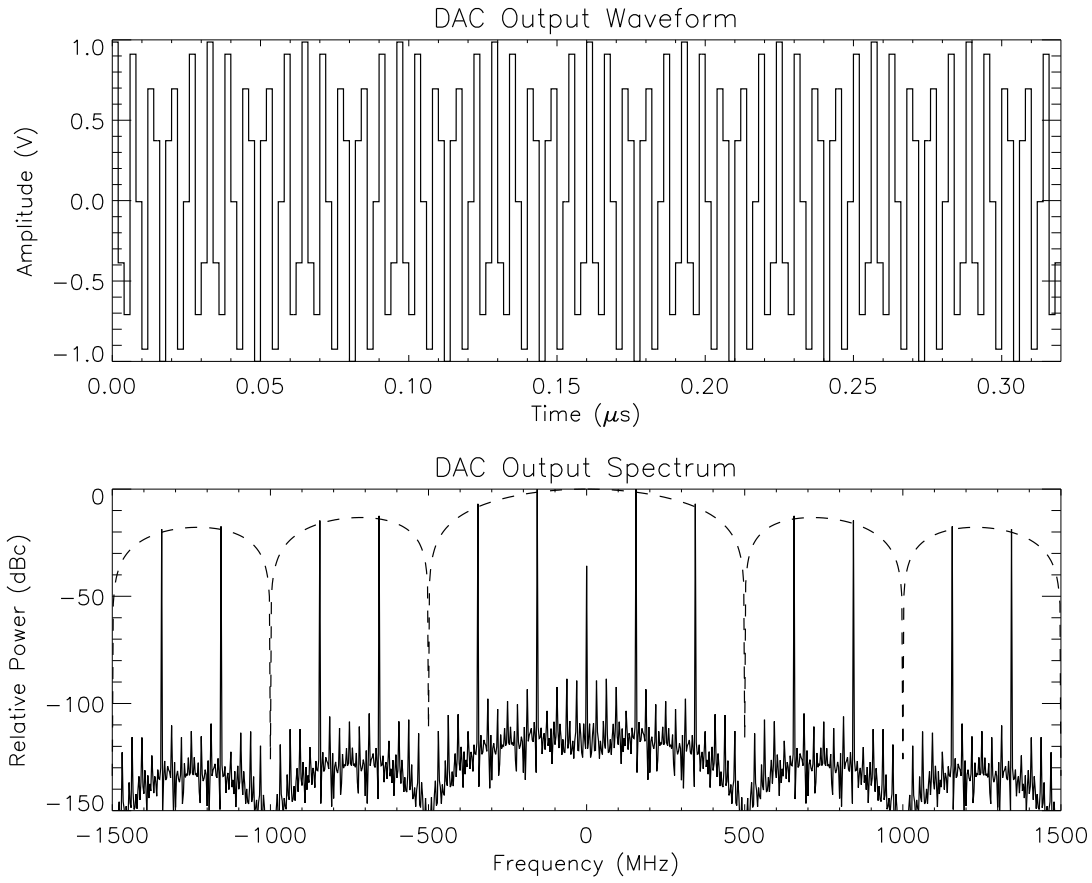

Figure 20: The top part of the figures shows the output waveform from the DAC of the signal at 156.25 MHz. The bottom part of the spectrum of the output signal from −1500 to 1500 MHz.

C Analysis of Alternate Intermediate Frequencies

Other intermediate frequency and sampling frequency combinations were considered. A analysis of a 75 MHz intermediate frequency and 100 MS/s sampling frequency is presented to illustrate a case below the Airband frequency range.

An intermediate frequency of 75 MHz and a sampling frequency of 100 MS/s (DAC and ADC clock frequency) satisfy the $f_s/4$ sampling criterion. However, the spurious signals generated by this combination are worse than for the combination proposed in the Section A.

To generate a signal at a center frequency of 75 MHz, an interpolation factor of at least two is required. For an interpolation factor of two (DAC mode `X2/FMIX/QMIX`), the output sampling frequency

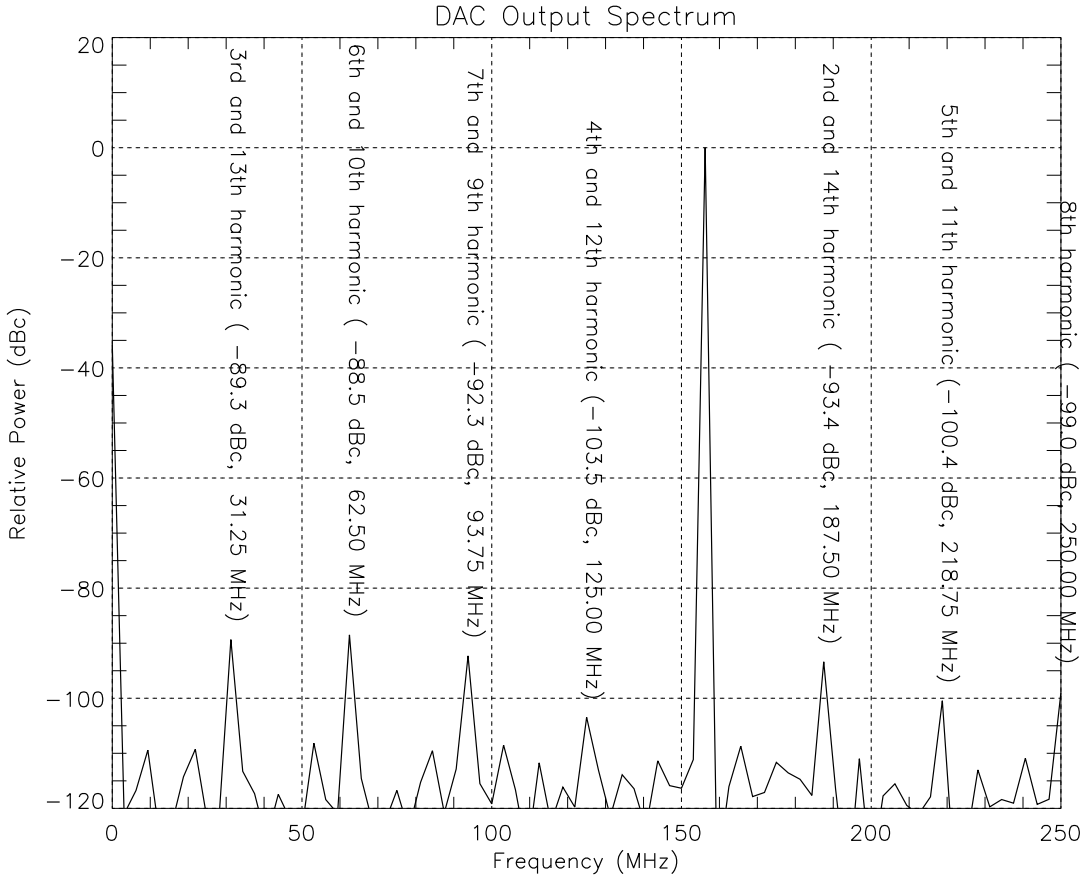

Figure 21: The spectrum of the output waveform between 0 and 250 MHz shown in Figure 20. The first 15 harmonics of the output signal are shown.

Table 6: DAC harmonics due to the DAC non linear conversion

Harmonic	**Frequency**	**Aliased**	
		+	−
	MHz	MHz	MHz
1	±156.25	156.25	−156.25
2	±312.50	−187.50	**187.50**
3	±468.75	−31.25	31.25
4	±625.00	**125.00**	−125.00
5	±781.25	−218.75	218.75
6	±937.25	−62.50	62.50
7	±1093.75	93.75	−93.75
8	±1250.00	250.00	−250.00
9	±1406.25	−93.75	93.75
10	±1562.50	62.50	−62.50
11	±1718.75	218.75	−218.75
12	±1875.00	−125.00	125.00
13	±2031.25	31.25	−31.25
14	±2187.50	**187.50**	−187.50
15	±2343.75	−156.25	**156.25**

is 200 MS/s, and a DAC-generated non-harmonic spurious signal ($f_{\mathrm{SIG}} - f_{\mathrm{DAC}}/2$) occurs at 25 MHz with a level of −30 dBc. Thus, there is 30 MHz between the upper and lower band edges of the spurious and desired signals, as opposed to 42.5 MHz for the 156.25 MHz/125 MS/s combination, and the spurious signal is 11 dB larger. In addition, the image frequency would be at 125 MHz, 50 MHz from the desired signal frequency, which would be hard to suppress sufficiently, and the seventh harmonic of the signal aliases back to 75 MHz.

For an interpolation factor of four, the course mixer cannot be used because it can only generate a local oscillator of $f_s/2 = 200$ MHz or $f_s/4 = 100$ MHz. Since the DAC fine mixer NCO maximum data rate is 320 MS/s, the signal could not be interpolated to the output sampling rate before up-conversion.. Therefore, the only mode that would work is `X4L/FMIX`. The NCO data rate would be 200 MS/s, and it would generate a 75 MHz local oscillator signal. In this mode, spurious signals exist at 25 MHz ($f_{\mathrm{SIG}} - f_{\mathrm{DAC}}/4$, −45 dBc) and 125 MHz ($f_{\mathrm{SIG}} - f_{\mathrm{DAC}}/2$, −37 dBc). As above, the band edge separation between the desired and spurious signals is 30 MHz for a 20 MHz band width signal, and the spurious signal levels are larger for this combination of intermediate frequency and sampling frequency than for the 156.25 MHz/125 MS/s combination.

The intermediate frequency cannot be generated directly without any DAC interpolation. The fine mixer NCO would need to run at 150 MS/s to generate a local oscillator of 75 MHz, which would mean that the input sampling rate would need to be 150 MS/s. However, the maximum clock frequency for the Model 7142 is 125 MHz.

In addition to DAC generated spurious signals that are easier to suppress, an intermediate frequency of 156.25 MHz also provides greater separation between the upper and lower side bands after up-conversion to the second stage intermediate frequency (312.5 MHz as opposed to 150 MHz). This greater separation allows the undesired side band to be suppressed by a greater amount or for a more linear phase filer pass band.

Finally, simulations show that the harmonics of the output signal generated by the non-linear conversion in the DAC are about the same levels in both cases. For all of these reasons, an intermediate frequency of 75 MHz and a sampling frequency of 125 MS/s was not selected.

C.1 LNA Gain and Noise Rise Analysis

The LNA gain significantly affects the noise power at the input to the analog to digital converter. To determine the appropriate LNA gain to use for the receiver, we can calculate the dynamic range of the receiver as a function of LNA gain and noise rise. Three LNA gains (20, 25, and 30 dB) are selected for this analysis. According to the manufacturer, the output power at the 1 dB compression point for the 20 dB gain LNA is −5 dBm and for the 30 dB gain LNA is −8 dBm. The 1 dB compression point for the 25 dB amplifier is computed by linear interpolation. Using this assumption, the output power at the 1 dB compression point for the 25 dB gain is −6.5 dBm.

In this analysis, ADC noise power is calculated by subtracting the ADC SNR (specified in the ADC data sheet) from the ADC -1dBFS power. The ADC SNR is a function of input signal frequency and sampling rate. For the LTC2255 (used on the Pentek Model 7142), the signal to noise ratio with a 156.25 MHz signal and a sampling rate of 125 MS/s is approximately 71.5 dB. The full scale input for this ADC is 10 dBm (2 Vpp) so -1dBFS is 9 dBm, and the noise power is -62.5 dBm. To ensure that quantization noise does not dominate, the level of the noise power at the input to the ADC must be

higher than the quantization noise power. For this analysis, I assume the quantization noise is equal to the noise power calculated from the ADC SNR. I define the difference between the quantization noise power and the noise power at the input to the ADC to be the noise rise.

Tables 7 to 10 show the results for the receiver noise level at 0, 3, 6, and 9 dB above the ADC noise power. The dynamic range only changes by 2.11 dB with the 30 dB LNA for all noise rise cases, whereas the dynamic range changes by 5.81 dB with the 20 dB LNA for all noise rise cases. Therefore, the 20 dB LNA provides more flexibility in compromising between dynamic range and mitigation of quantization noise.

Also, use of the 20 dB LNA provides for an increase in dynamic range by using a 16-bit ADC. For the LTC2209 (16-bit, 160 MS/s ADC), the signal to noise ratio with a 156.25 MHz signal and a sampling rate of 125 MS/s is approximately 76 dB. The full scale input for this ADC is 11 dBm (2.25 Vpp) so -1dBFS is 10 dBm. Therefore, the quantization noise power is -66 dBm. If a noise rise of 6 dB were used with this ADC, the receiver noise power must be -60 dBm at the input to the ADC. This case is very similar to the 3 dB noise rise case (Table 9) with the LTC2255, so the dynamic range would improve from 72.02 dBm to around 74.11 dB (approximately a 2 dB increase). Therefore, the 20 dB LNA provides the most flexibility in choosing an operating point for the receiver, and the best option for an upgrade in LNA.

Table 7: Receiver noise = −62.5 dBm (0 dB above ADC noise power).

				Values referenced to front-end		
LNA Gain	Atten 1	Atten 2	Noise power at ADC (20 MHz BW)	Receiver noise (4 MHz BW)	Max Input	Dynamic Range
dB	dB	dB	dBm	dBm	dBm	dB
30	−13	−13	−62.80	−99.99	−33.80	66.19
25	−11	−10	−62.71	−99.94	−30.30	69.64
20	−8	−8	−62.57	−99.86	−26.80	73.06

Table 8: Receiver noise = −59.5 dBm (3 dB above ADC noise power).

				Values referenced to front-end		
LNA Gain	Atten 1	Atten 2	Noise power at ADC (20 MHz BW)	Receiver noise (4 MHz BW)	Max Input	Dynamic Range
dB	dB	dB	dBm	dBm	dBm	dB
30	−12	−11	−59.87	−101.06	−33.80	67.26
25	−9	−9	−59.81	−101.02	−30.30	70.72
20	−7	−6	−59.67	−100.91	−26.80	74.11

Table 9: Receiver noise = −56.5 dBm (6 dB above ADC noise power).

				Values referenced to front-end		
LNA Gain	Atten 1	Atten 2	Noise power at ADC (20 MHz BW)	Receiver noise (4 MHz BW)	Max Input	Dynamic Range
dB	dB	dB	dBm	dBm	dBm	dB
30	−10	−10	−56.91	−101.72	−33.80	67.92
25	−8	−7	−56.86	−101.68	−30.30	71.38
20	−5	−5	−56.75	−101.58	−29.56	72.02

Table 10: Receiver noise = −53.5 dBm (9 dB above ADC noise power).

				Values referenced to front-end		
LNA Gain	Atten 1	Atten 2	Noise power at ADC (20 MHz BW)	Receiver noise (4 MHz BW)	Max Input	Dynamic Range
dB	dB	dB	dBm	dBm	dBm	dB
30	−9	−8	−53.94	−102.10	−33.80	68.30
25	−6	−6	−53.90	−102.06	−32.56	69.50
20	−4	−3	−53.78	−101.95	−32.56	69.39

References

[1] R. J. Doviak and D. S. Zrnić. *Doppler Radar and Weather Observations.* Academic Press, second edition, 1993.

[2] R. J. Hogan, N. Gaussiat, and A. J. Illingworth. Stratocumulus liquid water content from dual-wavelength radar. *J. Atmos. Oceanic Technol.*, 22(8):1207–1218, August 2005.

[3] H. J. Liebe, G. Hufford, and M. Cotton. Propagation modeling of moist air and suspended water/ice particles at frequencies below 1000 ghz. In *Proc. of 52nd Specialists meeting of the Electromagnetic Wave Propagation Panel*, page 542. AGARD, 1993.

[4] B. E. Martner,K. A. Clark, B. W. Bartram Radar Calibration Using a Trihedral Corner Reflector *Repr. fo 31st Conf. on Radar Meteorology*, page 1028-1030

[5] S. M. Sekelsky, E. E. Clothiaux Parallax Errors and Corrections for Dual-Antenna Millimeter-Wave Cloud Radars *J. Atmos. Oceanic Technol.*, Vol.19, p478-485, April 2002

[6] F. T. Ulaby, R. K. Moore, A. K. Fung Microwave Remote Sensing, Active and Passive *Artech House, Inc.*, Volume II, 1986

[7] M. I. Skolnik Introduction to Radar Systems *McGraw Hill Pub.*, third Edition, 2001

[8] Texas Instruments. *Understanding Data Converters*, 1995. Application Report.